AD-A188 469 ADVANCED ELECTRON OPTICS FOR VIBRATIONAL SPECTROSCOPY 1/1
(U) TEXAS UNIV AT AUSTIN DEPT OF PHYSICS J L ERSKINE
02 OCT 87 AFOSR-TR-87-1704 AFOSR-86-0291

UNCLASSIFIED F/G 20/14 NL

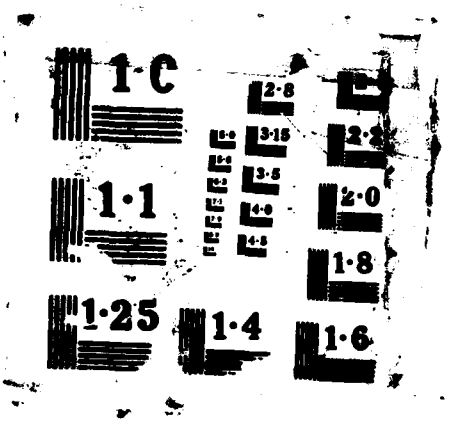
1·C
1·1
1·25
1·4
2·8
3·15
3·5
2·0
1·8
1·6

DTIC FILE COPY

UNCLASSIFIED
SECURITY CLASSIFICATION OF THIS PAGE

AD-A188 469

(2)

REPORT DOCUMENTATION PAGE

Form Approved
OMB No. 0704-0188

1a. REPORT SECURITY CLASSIFICATION Unclassified	1b. RESTRICTIVE MARKINGS None
2a. SECURITY CLASSIFICATION AUTHORITY	3. DISTRIBUTION/AVAILABILITY OF REPORT Approved for public release; Distribution unlimited.
2b. DECLASSIFICATION/DOWNGRADING SCHEDULE	
4. PERFORMING ORGANIZATION REPORT NUMBER(S) AFOSR-86-0291	5. MONITORING ORGANIZATION REPORT NUMBER(S) AFOSR-TR- 87-1704

DTIC ELECTE OCT 1 1987 S D

6a. NAME OF PERFORMING ORGANIZATION The University of Texas Department of Physics	6b. OFFICE SYMBOL (If applicable)	7a. NAME OF MONITORING ORGANIZATION Air Force Office of Scientific Research Chemical and Atmospheric Sciences
6c. ADDRESS (City, State, and ZIP Code) The University of Texas at Austin Department of Physics Austin, Texas 78712		7b. ADDRESS (City, State, and ZIP Code) Building 410 Bolling Air Force Base Washington, D.C. 20332-6448
8a. NAME OF FUNDING/SPONSORING ORGANIZATION AFOSR	8b. OFFICE SYMBOL (If applicable) NC	9. PROCUREMENT INSTRUMENT IDENTIFICATION NUMBER AFOSR-86-0291
8c. ADDRESS (City, State, and ZIP Code) Building 410 Bolling Air Force Base, Washington, D.C. 20332-6448		10. SOURCE OF FUNDING NUMBERS

PROGRAM ELEMENT NO.	PROJECT NO.	TASK NO.	WORK UNIT ACCESSION NO.
61102F	2917	A2	

11. TITLE (Include Security Classification)
Final Report - Unclassified
Advanced Electron Optics for ~~Di~~rational Spectroscopy

12. PERSONAL AUTHOR(S)
J.L. Erskine

13a. TYPE OF REPORT	13b. TIME COVERED	14. DATE OF REPORT (Year, Month, Day)	15. PAGE COUNT
Final	FROM 8-15-86 TO 8-14-87	1987 October 2	

16. SUPPLEMENTARY NOTATION

17. COSATI CODES			18. SUBJECT TERMS (Continue on reverse if necessary and identify by block number)
FIELD	GROUP	SUB-GROUP	

19. ABSTRACT (Continue on reverse if necessary and identify by block number)

The objective of this project is to develop an inelastic electron scattering spectrometer with significantly enhanced capabilities for studying physical and chemical phenomena at surfaces. The instrument combines off-the-shelf commercial instrumentation for sample preparation and characterization with a prototype state-of-the-art high resolution electron energy loss spectrometer (EELS) for studying vibrational properties of surfaces. The capabilities of this new instrument are unique. It extends the application of high resolution electron energy loss spectroscopy to include studies of technical surfaces such as polycrystalline surfaces, disordered thin films and non-single crystal alloy surfaces. Important applications are anticipated including studies of technical surfaces as alloys of aluminum and titanium. The new instrument also extends the range of vibrational spectroscopy studies of single crystals. Detailed tests of scattering selection rules and accurate measurements of the energy and angular dependence of inelastic electron scattering are now possible using the new instrument.

20. DISTRIBUTION/AVAILABILITY OF ABSTRACT	21. ABSTRACT SECURITY CLASSIFICATION
☒ UNCLASSIFIED/UNLIMITED ☒ SAME AS RPT. ☐ DTIC USERS	Unclassified

22a. NAME OF RESPONSIBLE INDIVIDUAL	22b. TELEPHONE (Include Area Code)	22c. OFFICE SYMBOL
Lt. Col. Larry Burggraf	(202) 767-4960	NC

DD Form 1473, JUN 86 — Previous editions are obsolete. — SECURITY CLASSIFICATION OF THIS PAGE

FINAL REPORT

ADVANCED ELECTRON OPTICS FOR VIBRATIONAL SPECTROSCOPY

J.L. Erskine
The University of Texas
Department of Physics
Austin, Texas 78712

24 September 1987

Final Technical Report
Reporting Period Ending 14 August 1987
Grant No. AFOSR-86-0291

Prepared for:

Air Force Office of Scientific Research
Directorate of Chemical and Atmospheric Sciences
Building 410
Bolling Air Force Base
Washington, D.C. 20332-6448

OBJECTIVE

The objective of this project is to improve the versatility and state-of-the-art sensitivity of Electron Energy Loss Spectroscopy (EELS) by two orders of magnitude. The projected improvements will permit several new classes of scientific studies based on vibrational spectroscopy including 1) analysis of chemical reactions (involving hydrogen in particular) with technical surfaces (polycrystalline metal alloy surfaces) and 2) accurate tests of inelastic scattering selection rules. In addition, the improvements in EELS electron optics will permit meaningful measurements of the energy and angle dependent inelastic electron scattering cross sections which will also test new theoretical predictions as well as yield information regarding the site location and orientation of chemical species on surfaces.

APPROACH

Our approach is to combine off-the-shelf commercial instrumentation for sample preparation and characterization with a prototype state-of-the-art high resolution electron energy loss spectrometer designed and constructed to optimize performance in conducting out of specular direction inelastic scattering experiments. The electron optics, control electronics and instrument goniometers are custom designed to suit the anticipated applications, and have been constructed in our shops and laboratory.

SUMMARY OF PROGRESS

A schematic drawing of our new spectrometer is shown in the accompaning figure. The vacuum system consists of two chambers separated by a gate valve, a long travel manipulator, and pumps. The vacuum system was assembled from standard pumps valves and hardware, and two custom designed chambers, one for sample preparation and characterization, and the second for housing the new EELS optics. The EELS optics chamber was fabricated to our specifications from mu-metal by Vacuum Generators in England.

The sample preparation/characterization chamber provides ports for low energy electron diffraction (LEED) optics, electron spectroscopy of surfaces based on electron, x-ray or ultraviolet sources, and mass spectroscopy analysis of desorbed species. Ports suitable for MBE sample synthesis, and for standard sample cleaning by sputtering are also available. The mu-metal chamber houses the EELS monochromator and analyzer which are separately mounted on their own manipulators. Separate mounting allows independent positioning of the monochromator and analyzer in orthogonal planes. This unique flexibility is required to perform experiments which test model calculations of inelastic scattering from oriented molecules on surfaces.

Our new EELS optics have been developed based on analysis of the characteristics of hemispherical analyzers (1) and electron raytracing studies (2) of several zoom lens configurations including 4-element zoom lenses. The configuration of the new multichannel detection analyzer is described in the appendix of this report. The current status of the major subsystems of the new EELS spectrometer is summarized below. We are projecting full operation of the instrument in January 1988.

Vacuum System: Complete and tested at 2×10^{-11} Torr.

Sample Characterization: LEED optics installed and tested; Auger analyzer, expecting delivery from Microscience; other systems including the mass spectrometer, sputter gun, and electron beam sample heater, have been installed and tested.

Monochromator: Shop work is complete and initial tests are complete. Target currents of $\sim 10^{-9}$ amps at 10meV resolution have been achieved. (This represents a significant improvement over our Leybold-Heraeus ELS-22 instrument).

Analyzer: Shop work is complete and initial tests of multichannel detector have been carried out. We have not yet been able to test the energy resolution. Monochromator and analyzer control units have been designed, built and tested to 350 volt kinetic energies. Noise levels are below one meV RMS on all sensitive outputs (to hemispheres, slits, terminators).

Computer Software: The assembly language driver required to transfer data from the position sensitive detector buffer memory to the computer has been written and tested. Some additional FORTRAN software is being developed.

Sample Manipulator: A standard commercial Z translation stage (UHV Instruments) has been adapted to the chamber; and a liquid nitrogen cooled probe arm is being constructed in our shop.

Monochromator Manipulator: Complete and tested.

Analyzer Manipulator: Final design complete, it is being built by our shop.

This new instrumentation is a build-from-scratch project which involves a number of highly complex subsystems requiring careful design backed in some cases by prototype testing and large scale numerical simulation (raytracing analysis). We have made excellent progress toward achieving our design objectives. We expect this instrument to be fully operational within six months.

REFERENCES

1. Refer to the paper by Hadjarab and Erskine (Publications and Appendix).

2. Refer to the paper by Strong and Erskine, the thesis by Sellidj and the paper by Erskine (Publications and Appendix).

PUBLICATIONS RELATED TO THIS PROJECT

Instrumentation Papers: (Copies of the three instrumentation papers are included in the Appendix).

R.L. Strong and J.L. Erskine, "A New Lens System for Surface Vibrational Spectroscopy at High Impact Energies", Rev. of Sci. Instruments 55, 1304 (1984).

F. Hadjarab and J.L. Erskine, "Image Properties of the Hemispherical Analyzer Applied to Multichannel Energy Detection", J. Electron Spect. Rel. Phen. 36, 227 (1985).

J.L. Erskine, "Advanced Electron Optics for Vibrational Spectroscopy", J. Electron Spect. Rel. Phen. 39, 265 (1986).

Selected Recent Scientific Papers (AFOSR supported) Based on EELS Techniques:

R. L. Strong and J. L. Erskine, "A Simple Lattice Dynamical Slab Model for Interpreting Surface Vibrational Spectra: Application to Oxygen on Ni(100) and Ni(111)", Phys. Rev. B31, 6305 (1985).

R. L. Strong and J. L. Erskine, "Adsorbate Structure Determination Using Surface Vibrational Spectroscopy", Phys. Rev. Lett. 54, 346 (1985).

J. L. Erskine, "High-Resolution Electron Energy Loss Spectroscopy: Explored Regions and the Frontier", J. Vac. Sci. Technol. A4, 1414 (1986).

J. P. Woods and J. L. Erskine, "High-Resolution Low-Energy Electron Reflection from W(100) Using the Electron Energy Loss Spectrometer: A Step Towards Quantitative Analysis of Surface Vibrational Spectra," J. Vac. Sci. Technol. 5, 435 (1987).

J. P. Woods, A. D. Kulkarni, J. L. Erskine and F. W. de Wette, "Vibrational Properties of β_1H and β_1D on W(001): Electron Energy Loss Measurements and Lattice-Dynamical Calculations," Phys. Rev. B30, xxxx (1987).

J. L. Erskine, "High Resolution Electron Energy Loss Spectroscopy," CRC Critical Reviews, CRC Press (1986). (Review Article, 85 pages).

PERSONNEL: (1984 - 1986)

R.L. Strong, Student (Ph.D. December 1984) Now at Texas Instruments Central Research Laboratories, Dallas.
Thesis Title: "Adsorbate Structure Determination Using EELS and Lattice Dynamical Calculations"

J.P. Woods, Student (Ph.D. December 1986) Now at M.I.T., Materials Science Department.
Thesis Title: "High-Resolution Electron Energy Loss Spectroscopy Studies of Clean and Hydrogen Covered Tungsten Surfaces"

Fawzi Hadjarab, Student (M.A. May 1984) Currently a Ph.D. candidate, UT Austin.
Thesis Title: "Image Properties of the Hemispherical Analyzer"

Abdelkrim Sellidj, Student (M.A. May 1984) Currently a Ph.D. candidate, UT Austin.
Thesis Title: "A Lens System for an EELS Energy Analyzer"

INTERACTIONS

Invited Talks (1984 - 1986) Related to EELS Spectroscopy

"Surface Vibrational Spectroscopy", 1984 High Energy Excitations in Condensed Matter Workshop", Los Alamos National Labs., Albuquerque, New Mexico, February 13-15, 1984.

"High Resolution Electron Energy Loss Study of Ordered Structures at Metal Surfaces", 20th Annual Symposium, The New Mexico Chapter of the American Vacuum Society, Albuquerque, New Mexico, April 17-19, 1984.

"High-Resolution Electron Energy Loss Spectroscopy: Explored Regions and the Frontier", J. L. Erskine, 32nd National Symposium of the American Vacuum Society, Houston, Texas, Nov. 18-22, 1985.

"Research in Surface Physics", J. L. Erskine Symposium on Surface Chemical Processes, Chemistry Dept., University of Texas, Austin, Oct. 3, 1985.

"Electron Energy Loss Studies of Chemisorbed Underlayers at Metal Surfaces", J. L. Erskine, Department of Chemistry, University of Wisconsin, Madison, Wisconsin, Oct. 23, 1986.

"Surface Vibrations on Clean and Hydrogen Saturated W(100)," J.L. Erskine, J.P. Woods, A.D. Kulkarni and F.W. de Wette, Vibrations at Surfaces V, Eibsee Hotel, D-8104 Grainau-Eibsee, Fed. Rep. Germany, Sept. 6-10, 1987.

SEMINARS/CONFERENCES (1984 - 1986) RELATED TO EELS SPECTROSCOPY

"Surface Vibrational Spectroscopy of Ordered Overlayers on Crystal Surfaces", J.L. Erskine, American Vacuum Society Lecture, Texas A&M Unversity, College Station, Texas, April 24, 1984.

"Electron Energy Loss Studies of Ordered Structures at Metal Surfaces", J.L. Erskine, Physics Department Colloquium, UT Arlington, Arlington, Texas, February 22, 1984.

"Adsorbate Structure Determination Using Electron Energy Loss Spectroscopy and a Parametrized Lattice Dynamical Slab Model", R.L. Strong and J.L. Erskine, Forty-Fourth Annual Conference on Physical Electronics, Princeton, NJ, June 18-20, 1984.

"New Instrumentation for Studying EELS Impact Scattering Cross Sections", J. L. Erskine, Vibrations at Surfaces IV, Bowness-on-Windermere, England, Sept. 15-19, 1985.

"Surface Vibrational Resonances and the Order-Disorder Transformation at the W(100) Surface," J. P. Woods and J. L. Erskine, 32nd National Symposium of the American Vacuum Society, Houston, Texas, Nov. 18-22, 1985.

"High Resolution Electron Energy Loss Spectroscopy of Surface and Subsurface Adsorbate Complexes", J. L. Erskine, AFOSR Conference on Chemical Dynamics, Dayton, Ohio, November 4-6, 1985.

"High Resolution Electron Energy Loss Spectroscopy Studies of the Interaction of H with Nb(100)", Y. Li, J. L. Erskine and A. Diebold, Bull. Am. Phys. Soc. 31, 272 (1986).

"High Resolution Low Energy Electron Diffraction Studies of W Using an Electron Energy Loss Spectrometer", J. P. Woods and J. L. Erskine, 33rd National Symposium of the American Vacuum Society, Boston, Massachusetts, Oct. 27-31, 1986.

"High Resolution Electron Energy Loss Spectroscopy of Adsorbates at Metal Surfaces," J. L. Erskine, Joint Meeting of the Texas Section of the APS and AAPT; Abilene Christian University, March 6-7, 1987.

"Vibrational Spectroscopy Studies of Hydrogen at Metal Surfaces," J.L. Erskine, AFOSR Surface Chemistry Contractors' Conference, Colorado Springs, Colorado, September 16-18, 1987.

MULTI CHANNEL DETECTION
ELECTRON ENERGY LOSS SPECTROMETER

SAMPLE HOLDER AND MANIPULATOR

- PRECISION LINEAR MOTION
- PRECISION ROTATION MOTION
- LIQUID NITROGEN COOLING
- ELECTRON BEAM HEATING

PREPARATION CHARACTERIZATION CHAMBER

- LEED/AES
- MASS SPECTROMETER
- MBE

ELECTRON SCATTERING CHAMBER

MONOCHROMATOR X-Y TABLE AND GONIOMETER

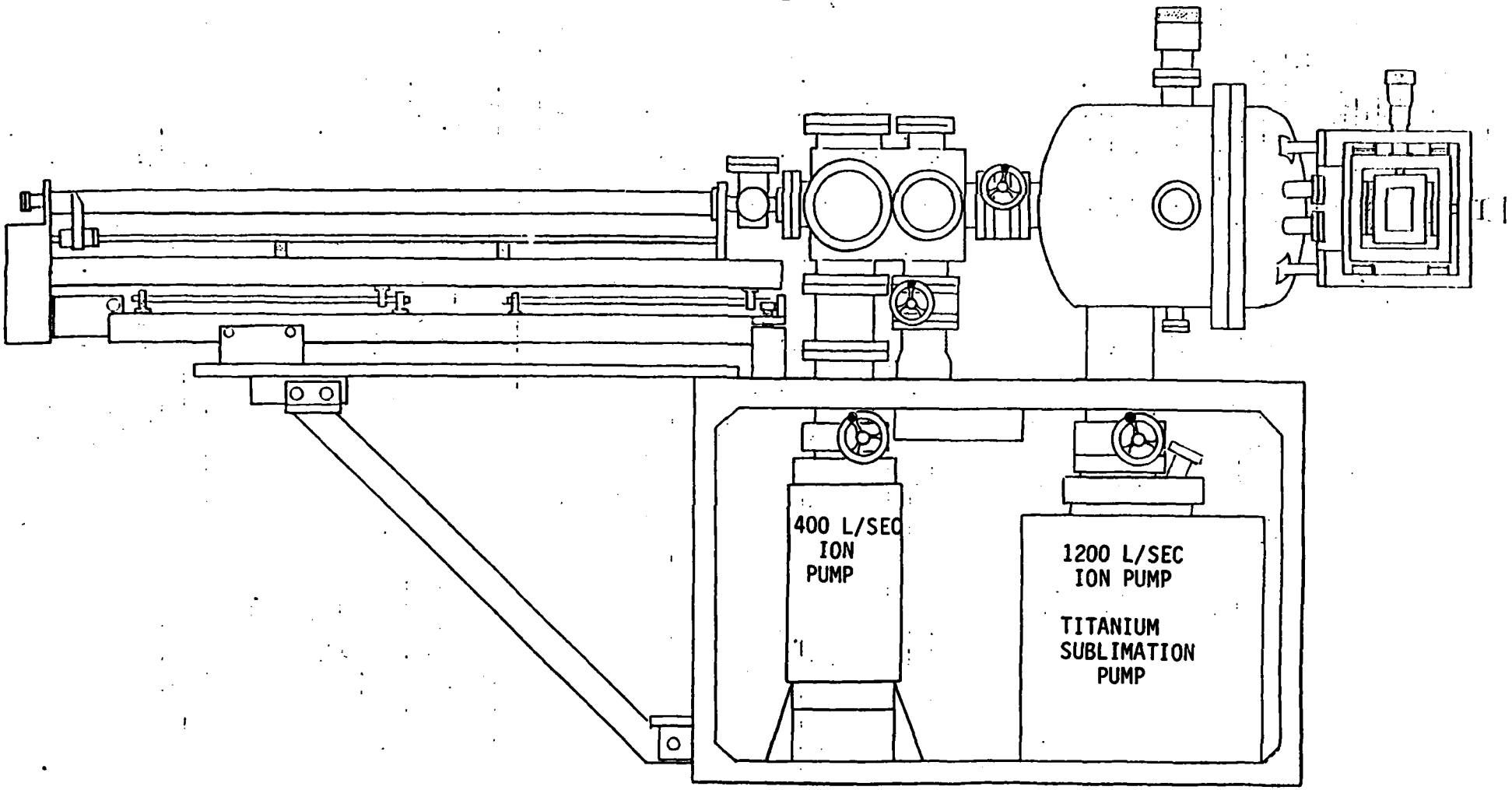

APPENDIX

Reprints Related to the New Instrumentation

1. New Lens System for Surface Vibrational Spectroscopy at High Impact Energies

2. Image Properties of the Hemispherical Analyzer Applied to Multichannel Energy Detection

3. Advanced Electron Optics for Vibrational Spectroscopy

New lens system for surface vibrational spectroscopy at high impact energies

R. L. Strong and J. L. Erskine

Department of Physics, University of Texas, Austin, Texas 78712

(Received 15 March 1984; accepted for publication 25 April 1984)

The design, characterization, and performance of a new lens system which permits high-resolution electron energy-loss spectroscopy (EELS) studies at high energies is described. The lens system can be adapted to most existing EELS instruments and extends the impact energy range to 300 eV. Electron ray-tracing techniques are used to characterize operating modes of one of the more common EELS optics designs as well as the new lens configuration. The results presented in this paper demonstrate some limitations of matrix optics approaches and the applicability of electron ray-tracing techniques for characterizing the transmission properties, angular profiles, image sizes, and operating modes of EELS spectrometers.

INTRODUCTION

High-resolution electron energy-loss spectroscopy (EELS) is rapidly becoming one of the most useful techniques for probing physical and chemical phenomena at surfaces. The EELS technique is based on detection of quantum energy losses in a monoenergetic electron beam scattered from a surface. Quantum energy losses (or gains) at surfaces result from excitations involving intrinsic surface vibrations (surface phonons) or vibrations of adsorbed atomic or molecular species. The technique combines high surface sensitivity (0.001 monolayer coverages can be detected in ideal cases) with a broad spectral range (good spectrometers are able to measure losses below 20 meV). In addition, EELS is one of the few surface sensitive techniques which can be considered a molecular spectroscopy rather than an atomic one.

The importance of studying vibrational properties of matter has been recognized for many years. Vibrational spectra provide information which is closely related to microscopic forces in matter and, in many cases, simple models and symmetry relations, in conjunction with vibrational data, can lead directly to important insight into the structure. This direct relationship between experimental data and molecular level physical parameters is one feature which seems to characterize the most useful spectroscopic probes.

Recent experimental results which combine EELS data with lattice dynamical calculations have emphasized the potential of using vibrational spectroscopy to investigate surface crystallography. EELS studies of the O/Al (111) system combined with lattice dynamical calculations have shown that surface complexes consisting of both overlayer and underlayer chemisorbed species can be investigated.[1] Similar investigations of the O/Ni (100) system have shown that EELS data combined with lattice dynamical models can be used to test structural models and adsorbate bond distances.[2,3] The dispersion of intrinsic surface phonon bands on Ni (100) has been recently measured using EELS.[4] Intrinsic phonon band mapping and detection of adsorbate vibrational modes having eigenvectors parallel to the surface generally require a nonspecular scattering configuration (refer to Fig. 1). In nonspecular scattering geometry, vibrational losses result from the impact scattering mechanism,[5,6] whereas vibrational losses observed using specular geometry are generally due to dipole scattering.[7]

The incident energy dependence of dipole scattering and impact scattering is different and, as will be discussed in the next section, the two scattering mechanisms differ in several other important aspects. In general, it is preferable to study dipole scattering vibrational losses at lower impact energies and impact scattering vibrational losses at higher impact energies. Most existing EELS spectrometers have been designed to study dipole vibrational losses. Therefore, the lens systems and control electronics typically permit electron scattering studies at energies up to 20 eV, but not at energies of several hundred electron volts which are often required for some impact scattering experiments.

This paper describes a straightforward lens system modification of one of the more common EELS spectrometer designs which permits operation of the spectrometer at impact energies above 300 eV. Electron ray-tracing techniques are used in the new lens design, and are also used to

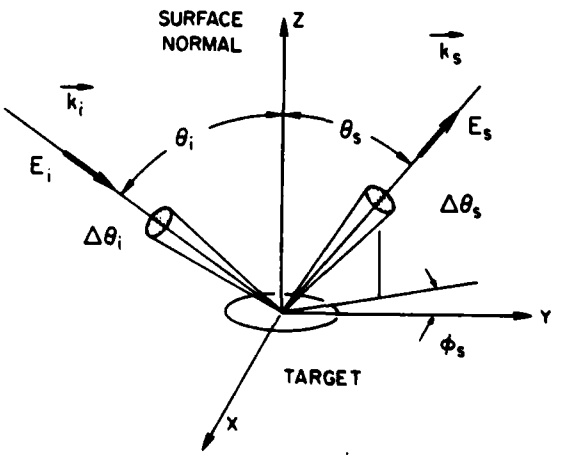

FIG. 1. Scattering geometry and parameters. Specular geometry $\theta_i = \theta_s$ and $\phi_s = 0$; off-specular geometry, $\theta_i \neq \theta_s$ or $\phi_s \neq 0$. E_i and E_s refer to incident and scattered electron energy. k_i and k_s are the electron incident and scattered wave vectors.

 0034-6748/84/081304-06$01.30

determine the beam profiles and image characteristics associated with spectrometer operating modes established empirically. (An operating mode consists of the set of lens voltages established by maximizing the counting rate for a given beam energy.) These studies have shown that ray-tracing is a valuable tool for understanding and optimizing the performance of high-resolution electron scattering optics.

I. ELECTRON SCATTERING MECHANISMS

To better understand the motivation for extending the scattering energy range of EELS spectrometers, it is helpful to briefly consider what has been established about electron scattering phenomena at surfaces. It is now well established that two distinct scattering regimes are required to account for experimental observations of vibrational losses measured by inelastic electron scattering from surfaces. The basic difference between these two regimes is that one is based on long-range dipolar fields which produce small-angle (forward) inelastic scattering,[7] and the other is based on short-range atomic-like fields which produce large-angle (diffuse) inelastic scattering.[5]

Vibrational losses observed using specular geometry (refer to Fig. 1) generally result from the "dipole" scattering mechanism.[7] In this scattering regime, the process is viewed as a combination of inelastic forward scattering by dipolar fields followed or preceded by elastic backscattering (reflection) from the surface. Dipole scattering is, therefore, characterized by a narrow angular spread around the specular scattering angle. A careful analysis of dipole scattering shows that due to the finite energy loss, two lobes appear on either side of the specular angle having an angular separation $\Delta\theta_s = \pm \Delta E/2E_i$, where ΔE is the energy loss and E_i is the incident energy. In addition, the dipole cross section integrated over these two forward scattering lobes is proportional to $E_i^{-3/2}$. This implies that one characteristic of dipole scattering is a ratio of loss peak intensity to elastic peak intensity which varies as $E_i^{-3/2}$, if the reflectivity of the crystal is a slowly varying function of energy.

A second and distinctly different scattering regime termed "impact" scattering is associated with short-ranged atomic-like potentials.[5] Electrons scattered by vibrational excitations in this regime exhibit a more isotropic angular spread.[6] In addition, the cross-section energy dependence is no longer a simple monotonic function of E_i and in fact contains structure which is related to bond distances and other surface crystallographic parameters.[5,8] The most striking difference between these two scattering mechanisms, from an experimental point of view, is the relative magnitude of the differential scattering cross sections. The total scattering cross section for impact scattering is comparable to (or larger than) dipole cross sections. However, under typical experimental conditions, when the energy analyzer defines a small acceptance cone (typically $\Delta\theta_s$ is 1° or less), the actual counting rate associated with the two scattering mechanisms is vastly different. For example, with a clean well-ordered crystal, state-of-the-art EELS spectrometers operating at 5-meV resolution yield elastic peak counting rates in specular geometry of about 10^5 Hz. A dipole loss feature measured using monolayer coverages will yield typical counting rates,

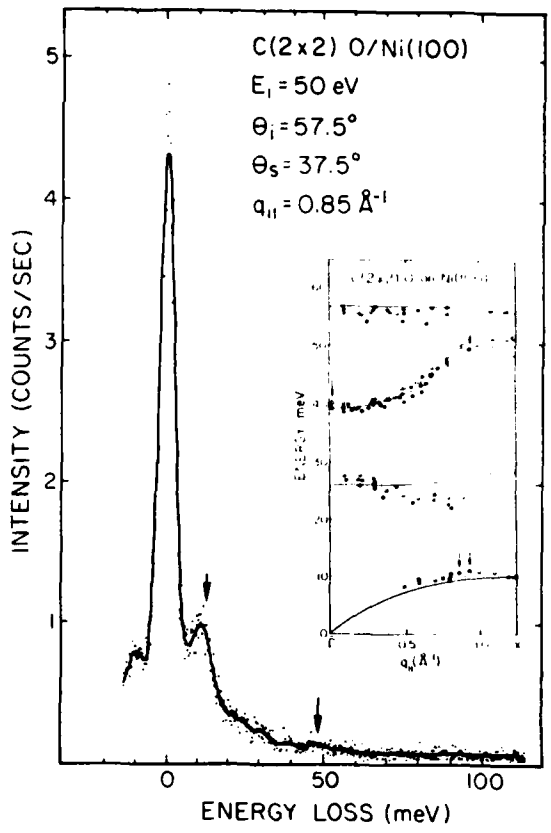

FIG. 2. EELS spectra for $c(2\times2)$O/Ni (100) taken in off-specular geometry at 50-eV impact energy. Inset illustrates calculated surface phonon bands along the $\bar{\Delta}$ line (Ref. 2). Open circles, data from Ref. 3, solid circles from Ref. 2. Points in inset indicated by arrows correspond to data for spectra illustrated in this paper.

under the same conditions, of a few hundred Hz, and an impact loss peak, observed under corresponding conditions, will yield a counting rate of the order of 1 Hz or less.

Energy and momentum conservation associated with the excitation of a phonon having energy $\hbar\omega$ require

$$E_i = E_s + \hbar\omega, \tag{1}$$

$$\mathbf{k}_i \sin\theta_i = \mathbf{k}_s \sin\theta_s + \mathbf{q}_{\parallel} + \mathbf{G}, \tag{2}$$

where $\mathbf{G}$ is a two-dimensional reciprocal lattice vector (usually 0) and $\mathbf{q}_{\parallel}$ is restricted to the first surface Brillouin zone. If θ_i and θ_s are the incidence and scattering angles measured from the surface normal, $|\mathbf{q}_{\parallel}|$ is given by

$$|\mathbf{q}_{\parallel}| = \frac{2m_e}{\hbar}|\sqrt{E_i}\sin\theta_i - \sqrt{E_i - \hbar\omega}\sin\theta_s| \tag{3}$$

or, if $\hbar\omega \ll E_i$,

$$|\mathbf{q}_{\parallel}| = 0.512\sqrt{E_i(\text{eV})}|\sin\theta_i - \sin\theta_s|\text{Å}^{-1}. \tag{4}$$

From these equations, it is clear that independent of factors related to scattering cross sections, fairly high scattering energies are desirable to probe vibrational properties of the full surface Brillouin zone of a crystal surface. For example, the zone edge ($\bar{M}$ point) along the (11) direction ($\bar{\Sigma}$ line) of Ni (100) corresponds to $|\mathbf{q}_{\parallel}| = 1.785$ Å^{-1}. Choosing $\theta_s = 40°$ and $\theta_i = 60°$ as typical scattering angles, one finds that E_i must be about 240 eV to probe phonon modes at the zone edge. Mapping dispersion curves also requires a well-

defined analyzer acceptance angle to achieve a well-defined value of $|\mathbf{q}_{\parallel}|$. From Eq. (4), one obtains, for $\theta_i \neq \theta_s$,

$$|\Delta \mathbf{q}_{\parallel}| = |\mathbf{q}_{\parallel}| \left(\frac{\Delta E_i}{2E_i} + \frac{\Delta\theta_i \cos\theta_i + \Delta\theta_s \cos\theta_s}{|\sin\theta_i - \sin\theta_s|} \right). \quad (5)$$

Thus, it is apparent that higher impact energies help maintain accurate control over $\Delta q_{\parallel}$. It turns out that smaller values of $\Delta\theta_i$ and $\Delta\theta_s$ are more conveniently achieved at higher energies because of fundamental constraints associated with electron trajectories in nondispersive electron optical systems. These considerations help rationalize the need for increasing the energy of EELS spectrometers.

Figure 2 illustrates the use of the conservation laws to obtain one point of the S_4 surface phonon dispersion curve for $c(2\times2)$O/Ni (100) along the $\bar{\Gamma}$–$\bar{X}$ direction. The loss spectra was taken at 50-eV impact energy and using 20° off-specular scattering geometry. The parameters correspond to $|\mathbf{q}_{\parallel}| = 0.85$ Å^{-1}. These scattering parameters yield a strong elastic peak signal and pronounced gain and loss peaks 11 meV either side of the elastic peak corresponding to excitations involving the S_4 surface phonon of $c(2\times2)$O/Ni (100). The energy loss from the EELS data is plotted (with other data) on the inset which shows the calculated E vs $\mathbf{q}_{\parallel}$ dispersion of the S_4 and other oxygen-derived surface phonons for $c(2\times2)$O on Ni (100).[2] The spectra in Fig. 2 also exhibits evidence for additional modes of the $c(2\times2)$O/Ni (100) surface as indicated by an arrow on the spectrum and on the calculated phonon bands. These modes are more apparent at other impact energies.

II. ELECTRON OPTICS

Figure 3 illustrates the basic features of a typical EELS spectrometer which consists of an electron source and monochromator, acceleration and deceleration lenses, an energy analyzer, and a detector. Many variations are possible in implementing a working instrument; designs have been reported based on spherical (SDA-180°),[10] cylindrical (CDA-127°),[11] and cylindrical mirror (CMA-42°)[12] dispersive elements. The CMA-42° geometry is more cumbersome than the other two configurations for angle-dependent measurements and, in this paper, only the other two configurations, which are compatible with the illustration in Fig. 3, are considered. The discussion in the present paper centers on the lens systems in relation to the range of impact energies accessible and the angular considerations related to Eq. (5). Other technical considerations for both spherical (SDA-180°) and cylindrical (CDA-127°) EELS instruments, such as factors relating to resolution and counting rates, have been considered previously.[13]

The impact energy of electrons hitting the target is basically the monochromator pass energy plus the voltage difference between the exit slit and the target. The energy loss of analyzed electrons is basically the voltage difference between the monochromator and analyzer slits, assuming each analyzer is operating at the same pass energy. The input and output lenses do not affect the impact energy or the energy of analyzed electrons; however, they perform a critical function: they control the imaging properties of the spectrometer. Without suitable lens systems the intensity of detected signals would be too weak for useful spectroscopic work.

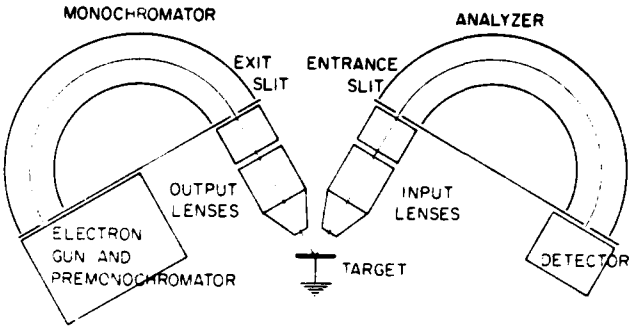

FIG. 3. Typical EELS spectrometer.

In arriving at a suitable lens system for a particular application, one of the most important considerations is the maximum acceleration and deceleration ratios which must be achieved. EELS measurements require energy resolution of the order of 5 meV. Various constraints related to magnetic shielding, size of the vacuum chamber, etc., have been considered in arriving at the physical dimensions and pass energies used in existing EELS optics. Typical instruments employ mean radii of a few centimeters, slit widths of a few tenths of a millimeter, and pass energies in the range of 0.2–2 eV. Instruments which are used primarily to study dipole losses are designed for impact energies in the 1–20 eV range. Higher energies are not necessary because dipole cross sections decrease with increasing energy. Impact energies of tens of electronvolts and pass energies of a few electronvolts or less require deceleration ratios of only a factor of 10. A single lens is capable of this range of deceleration ratio, and a three element zoom lens can accommodate a ratio of 15 while maintaining fairly good magnification characteristics.

When one considers the effect of requiring a deceleration ratio of 400 (this is the deceleration ratio needed to achieve 5-meV resolution using the same monochromator/analyzer configuration at 200–300 eV) it becomes apparent that this large deceleration ratio cannot be accomplished effectively in one stage. A single lens providing such a large deceleration ratio produces an image inside the lens field. The only suitable solution is a multistage lens system with one or more real images between the source and slit.

There are several possible approaches which can be adopted in extending the energy range of an existing EELS spectrometer. Three possibilities are: (1) redesign the entire lens system for the expanded energy range, (2) attempt to find suitable operating voltages which yield reasonable performance of the existing lens configuration, and (3) add some new lenses to the existing configuration. After some considerations based on general properties of electron optics and the characteristics of existing lens configurations of proven design, we decided that the third option presented the most attractive alternative. Option (2) can work in spectrometers having two or more lenses but, in our case, this option presented difficulty in terms of the new range of lens voltages required at high impact energies. This option would have required major changes in the existing control electronics.

Option (3) achieves a result which is nearly equivalent to the best result which would be expected from option (1) assuming the total number of lenses in each case is equal. Also, option (3) results in a design which maintains the original operating modes (lens voltages) by simply grounding the added lenses. The required lens voltages for the original lenses remained within the range available from the existing control unit, even when the optics are operated at 300-eV impact energy. This feature is a very convenient result of the design exercise. Essentially, we have shown that the addition of an extra lens can permit a factor of 15 increase in the energy range of EELS spectrometers while maintaining the energy resolution. No change in the voltage range of other spectrometer elements is required as long as the target can be operated at voltages different from ground potential.

III. NEW LENS CONFIGURATION

Figure 4 illustrates a cross-sectional view (in the scattering plane) of our old and new lens configurations. Our EELS spectrometer is a commercial tandem spectrometer (Leybold ELS-22) which is based on a pair of cylindrical analyzers (CDA-127°) and two element acceleration/deceleration lenses. The primary 127° sectors and lens systems are very similar to most of the single sector instruments[11] which have been constructed in various laboratories, and the lens system we have developed should function well on all of these instruments.

Most EELS spectrometers employ a circular electrostatic shield around the target to produce a field-free region near the scattering center. Electron acceleration and retardation are accomplished between lens elements which produce axial acceleration and focusing. Some spectrometers employ tube lenses (rotationally symmetric) and others employ lenses with rectangular apertures. The primary difference in these two lens configurations is that the rectangular lenses accommodate rectangular images slightly better, i.e., they tend to reduce chromatic aberrations along the major axis of a rectangular image. A three-element tube lens system with similar magnification properties should perform just as well as the rectangular lens system shown in Fig. 4.

In Fig. 4, existing components including lenses and the electrostatic shield are shown as solid lines; the new lens and shield are shown as dotted lines. The figure is drawn to scale, and the actual physical size is indicated by a 1-cm calibration mark. The original and new lens systems for the monochromator and analyzer sides of the spectrometer are identical; therefore, Fig. 4 illustrates only one side of the spectrometer optics. All three lenses of the monochromator and lenses L_1 and L_3 of the analyzer are split to provide beam steering capabilities. Lenses L_2 and L_3 are split parallel to the slit, L_1 is split perpendicular to the slit.

Our spectrometer had been operated for about 2 years before we added the new lenses, and we had established empirically, by tuning the instrument numerous times, a number of operating modes for resolutions ranging from 5 to 15 meV. We planned to use electron ray-tracing analysis to investigate the properties of the new lens system, and decided

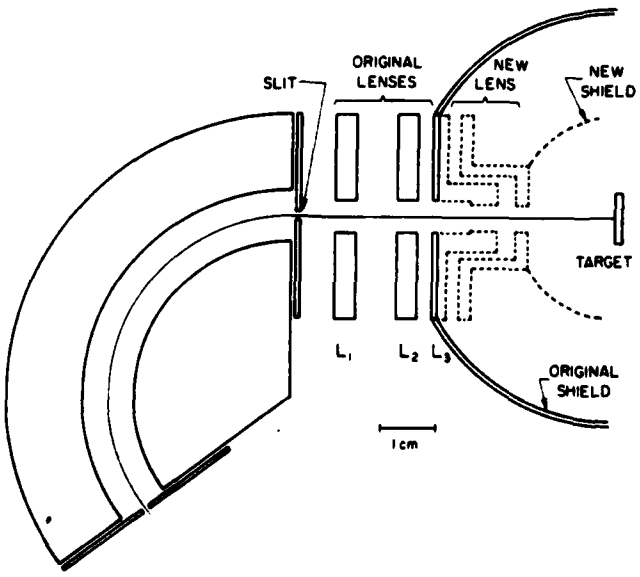

FIG. 4. Cross-sectional view of original (solid lines) and new lens system (dotted lines).

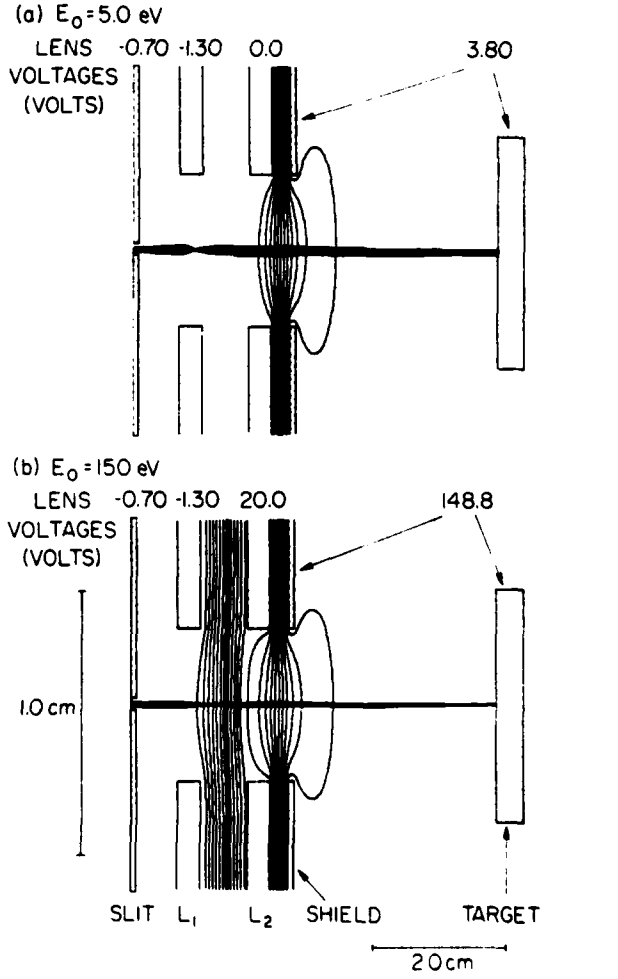

FIG. 5. Typical ray-tracing results for operating modes of the original lens system at two impact energies: (a) $E_i = 5$ eV; (b) $E_i = 150$ eV. Note difference between x and y scales.

to first apply these methods to the existing lens configuration with lens potentials specified by the voltages which had been established empirically.

The ray-tracing program we have used is a general-purpose program for computing fields and electron trajectories (W. B. Hermannsfeldt, S. L. A. C., Stanford University, 1973). We have used this program previously for developing an angle resolving photoelectron spectrometer,[14] and others have used it to evaluate input lens performance of a commercial ESCA spectrometer.[15] The program can accommodate either axial symmetric systems (i.e., a sequence of tube lenses), or systems having two-dimensional geometry (infinite extent in one dimension). We have found that ray-tracing results using either geometry can account for lens system behavior in applicable cases. We have conducted extensive ray-tracing studies of the tube lens system on our photoemission analyzer (using the axial symmetry program option) and of the original configuration of our EELS optics (using the two-dimensional program option). These studies have shown that ray-tracing results can be reconciled with empirical tests.[14]

Figure 5 displays ray-tracing results for two 10-meV resolution modes of the original lens configuration. Shown in the figures are the monochromator exit slit, the two lenses, L_1 and L_2, the electrostatic shield, and the target. Figure 5(a) corresponds to 5-eV impact energy, and the equipotentials are shown for multiples of 8% of the acceleration voltage. Figure 5(b) corresponds to 150-eV impact energy, and in this case two sets of equipotentials are shown, each set corresponding to 8% of the acceleration voltage of each lens. Clearly, L_2 is the stronger lens. Referring to Fig. 5(b), one can observe that equipotential lines extend into the "field-free" region, and that L_2 affects the properties of L_1. Geometrical optics approximations and matrix optics methods would not provide accurate results in this particular instance.

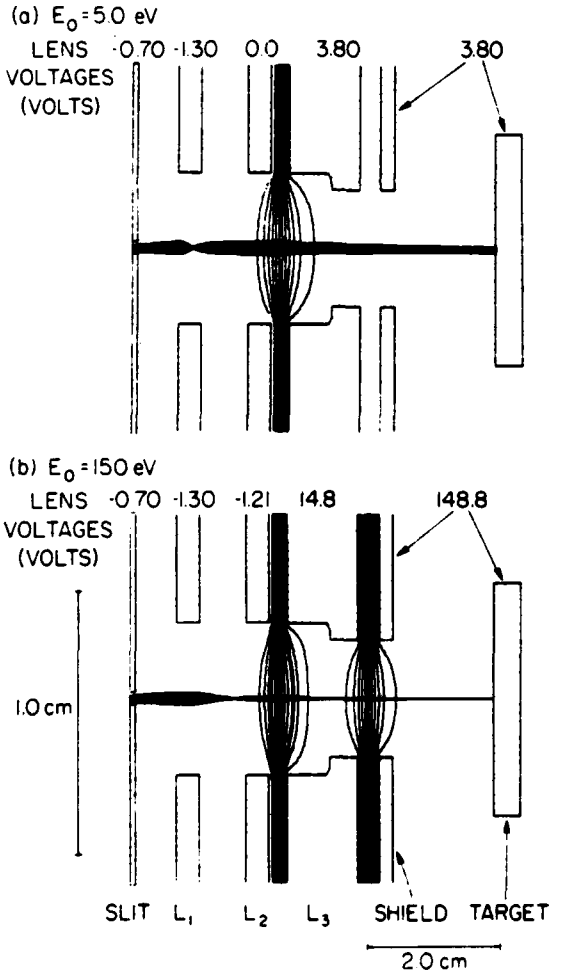

FIG. 6. Typical ray-tracing results for operating modes of the new lens system at two impact energies: (a) $E_i = 5$ eV; (b) $E_i = 150$ eV. Note difference between x and y scales.

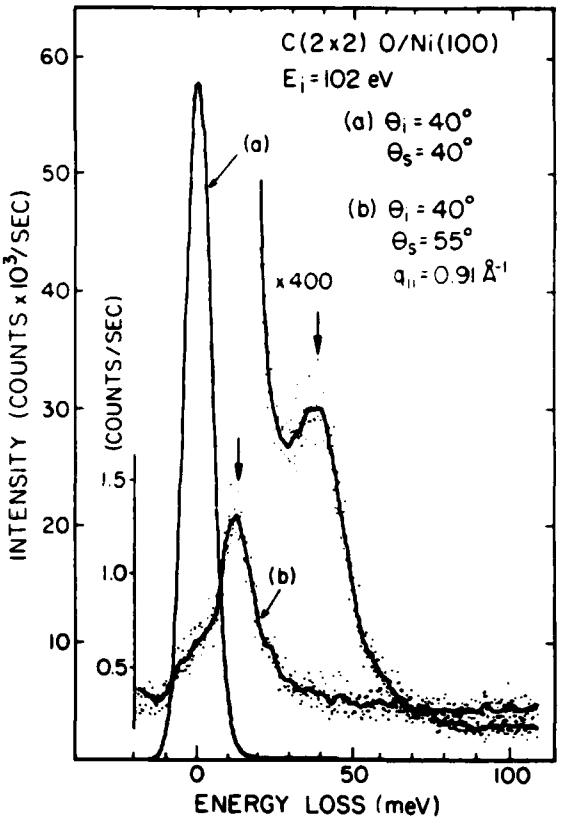

FIG. 7. EELS spectra for $c(2\times2)$O/Ni(100) at 102-eV impact energy. Curve (a) elastic peak and perpendicular oxygen vibrational loss peak observed in specular geometry. Curve (b) S_4 surface phonon peak observed in off-specular geometry. Note the elastic peak in curve (b) appears as only a shoulder.

Assumptions which were made in all of our EELS optics ray-tracing studies were: (1) the electrons emerged from the slit with kinetic energy equal to the pass energy (which is related to the slit potential), (2) the flux of electrons from the slit was uniform over the slit area and over an angular range which is limited by resolution considerations, and (3) the source area used when ray tracing electrons from the target to the analyzer was the area established by ray tracing from the monochromator to the target. The target area illuminated by the monochromator can also be estimated using the Helmholtz–Lagrange equation[14] based on assumptions (1) and (2), the accelerating potential, and the required angular resolution.

A number of ray-tracing studies of the original lens configuration (similar to the two cases shown in Fig. 5) estab-

lished that the modes which had been found empirically (by tuning the optics) correspond to beam profiles similar to those shown in the figure. The "correct" modes all seem to yield a narrow beam of electrons incident on the target, an image size comparable to the exit slit (near unity magnification), and a focal point near the plane of the lens nearest the slit. At low impact energies, as indicated in Fig. 5(a), most of the acceleration and deceleration of the beam occurs between the electrostatic shield and L_2.

Analogous ray-tracing studies of the new lens system based on voltages established by tuning the instrument were carried out to characterize operating modes at high impact energies. Figure 6 illustrates results for two modes corresponding to the same impact energies as for Fig. 5. Again, lens voltages which yield the best intensity at a given energy resolution yield a focal point near the plane of the lens nearest the slit. Notice that the 150-eV mode for the new lens system requires much lower L_1 and L_2 voltages compared with the corresponding voltages of the original lens configuration. Although not immediately apparent from Figs. 5 and 6, the 150-eV mode with three lenses has an angular spread one-fourth the value for the two lens system. This improves the $\Delta q_{\parallel}$ resolution according to Eq. (5). Also, note that in the three lens configuration the potential lines do not penetrate the electrostatic shield as in the case of the two lens configuration.

When the new lens and target are connected to ground, the spectrometer operating modes are very nearly equivalent to the modes which were established prior to the lens modification, and the resolution and intensity of the instrument were not affected by the new lens system over the range where performance can be compared.

Figure 7 illustrates spectra for $c(2\times2)O/Ni\ (100)$ obtained using the new lens system. Curves labeled (a) correspond to spectra taken at 102-eV impact energy in specular geometry ($\theta_i = \theta_s = 40°$). The loss peak at ~ 38 meV is produced by dipole scattering from the $O_\perp$ mode. Curve (b) corresponds again to the S_4 surface phonon of Ni (100) as shifted by the presence of $c(2\times2)$ oxygen. Note that the elastic peak intensity in this case ($\Delta\theta = 15°$) is reduced to a small shoulder to the left of the impact loss peak. There is no evidence of the $O_\perp$ mode in curve (b). These spectra clearly illustrate how impact scattering can be used to discriminate between dipole and impact loss structures in EELS spectra. The results of Fig. 7 are also plotted on the surface bands which appear as an inset in Fig. 2.

We have designed and tested a new lens system which permits high-resolution electron energy-loss spectroscopy measurements at high impact energies (several hundred eV). Our ray-tracing analysis of the original and new lens configurations has established the beam profiles and other beam parameters associated with one of the more popular EELS spectrometer configurations. The ray-tracing studies have also shown that operating modes established empirically by tuning EELS spectrometers (having real slits) for maximum intensity correspond to desirable beam properties including a small image at the target, small angular divergence, and efficient beam focusing at the monochromator entrance slit. Application of EELS at high impact energies has been demonstrated by mapping the surface phonon bands of $c(2\times2)O/Ni\ (100)$ along the $\overline{\Delta}$ line of the surface Brillouin zone.

ACKNOWLEDGMENT

This work was sponsored by the Air Force Office of Scientific Research under Grant No. AFOSR-83-0131.

[1] R. L. Strong, B. Firey, F. W. deWette, and J. L. Erskine, Phys. Rev. B 25, 5547 (1982).
[2] R. L. Strong and J. L. Erskine (to be published).
[3] J. M. Szeftel, S. Lehwald, H. Ibach, T. S. Rahman, J. E. Black, and D. L. Mills, Phys. Rev. Lett. 51, 268 (1983).
[4] S. Lehwald, J. M. Szeftel, H. Ibach, T. S. Rahman, and D. L. Mills, Phys. Rev. Lett. 50, 518 (1983).
[5] S. Y. Tong, C. H. Li, and D. L. Mills, Phys. Rev. Lett. 44, 407 (1980).
[6] W. Ho, R. F. Willis, and E. W. Plummer, Phys. Rev. B 21, 4202 (1980).
[7] E. Evans and D. L. Mills, Phys. Rev. B 5, 4126 (1971).
[8] G. C. Aers, T. B. Grimley, J. B. Pendry, and K. L. Sebastian, J. Phys. C 14, 3995 (1981).
[9] R. E. Allen, G. P. Alldredge, and F. W. deWette, Phys. Rev. B 4, 1661 (1971).
[10] J. E. Demuth, K. Christman, and P. N. Sanda, Chem. Phys. Lett. 76, 201 (1980); N. R. Avery, Appl. Surf. Sci. 13, 171 (1982); G. E. Thomas and W. H. Weinberg, Rev. Sci. Instrum. 50, 497 (1979).
[11] L. L. Kesmodel, J. Vac. Sci. Technol. A 1, 1456 (1983); M. Nishijima, S. Masuda, H. Kobayashi, and M. Onchi, Rev. Sci. Instrum. 53, 790 (1982); B. A. Sexton, J. Vac. Sci. Technol. 16, 1033 (1979); H. Ibach and D. Bruchmann, Phys. Rev. Lett. 41, 958 (1978); H. Ehrhardt, L. Langhans, F. Linder, and H. S. Taylor, Phys. Rev. 73, 222 (1968).
[12] S. Andersson and M. Persson, Phys. Rev. B 24, 3659 (1981).
[13] D. Roy and J. D. Carette, in *Electron Spectroscopy for Surface Analysis*, edited by H. Ibach (Springer, Berlin, 1977).
[14] G. K. Ovrebo and J. L. Erskine, J. Electron Spectrosc. Relat. Phenom. 24, 189 (1981); H. A. Stevens, A. W. Donoho, A. M. Turner, and J. L. Erskine, *ibid.* 32, 327 (1983).
[15] P. J. Orders, M. Sagurton, and C. S. Fadley, J. Electron Spectrosc. Relat. Phenom. (in press).

Journal of Electron Spectroscopy and Related Phenomena, 36 (1985) 227—243
Elsevier Science Publishers B.V., Amsterdam — Printed in The Netherlands

IMAGE PROPERTIES OF THE HEMISPHERICAL ANALYZER APPLIED TO MULTICHANNEL ENERGY DETECTION

F. HADJARAB and J.L. ERSKINE

Department of Physics, University of Texas, Austin, TX 78712 (U.S.A.)

(First received 13 September 1984; in final form 12 February 1985)

ABSTRACT

Electron trajectories through a hemispherical analyzer are studied in relation to applications using high spatial resolution position sensitive devices for multichannel detection. Criteria are established for optimizing detection efficiency, choosing various parameters and analyzing effects of fringing electric fields and magnetic fields on analyzer performance.

INTRODUCTION

Recent developments in low-distortion imaging detectors offer opportunities to improve substantially electron spectroscopic techniques in applications where low counting rates are the primary limitation. High-resolution electron imaging detectors based on a low distortion resistive anode coupled to a pair of multichannel plates have been developed by several groups [1—5], and a commercial detector based on this scheme is now available which achieves spatial resolution in excess of 100 line pairs over a one-inch diameter active area [6]. Applications using various types of imaging detectors are beginning to appear. Typical applications include low energy electron diffraction [7], photoelectron spectroscopy [8, 9], mass spectroscopy [10], and ion microscopy [11].

In applications requiring high energy resolution in directionally sensitive spectrometers (such as in angle-resolved photoemission, and high-resolution electron energy loss spectroscopy) a hemispherical analyzer is the best choice. This is because a properly designed input lens system can optimize the spectrometer étendue (the product of source area and solid angle) of a hemispherical analyzer so that it exceeds other analyzers which are suitable for directional detection [12]. In addition, the hemispherical analyzer exhibits first order stigmatic focusing characteristics which are important for detection schemes based on imaging detectors.

0368-2048/85/$03.30

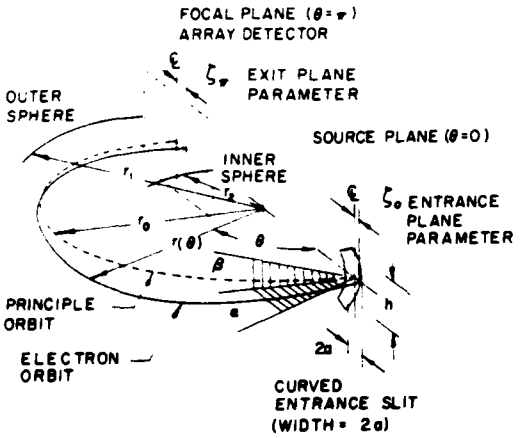

Fig. 1. Illustration of the parameters required to describe a hemispherical analyzer. Cross section in plane of principle electron orbit contains dashed line at r_0 (mean radius); r, θ, represent coordinates of an electron along a particular orbit (solid line); ζ_0 (ζ_π) represent displacements of electron from r_0 at entrance slit (exit plane). α, angle of electron velocity measured from principle orbit at entrance slit in the central orbit plane; β, corresponding angle at the entrance slit plane measured perpendicular to the central electron orbit.

The objective of the present paper is to present a comprehensive description of the properties of a hemispherical analyzer which have a bearing on applications that can utilize effectively multichannel detection. Our discussion includes analysis of the electron trajectories between the hemispheres, the imaging properties, optimization of the analyzer étendue and the effects of fringing electric fields and stray magnetic fields on analyzer performance. As a specific example, we present the analysis of an analyzer with high angular resolution designed to achieve 5 meV energy resolution at 2 eV pass energies and which is intended to be used with multichannel detection. Such an analyzer would be suitable for high-resolution, angle-resolved photoemission studies of solid surfaces, in high-resolution electron energy loss experiments, or selected gas phase photoemission studies.

ELECTRON TRAJECTORY THEORY

First we present an exact formulation of the electron trajectories and imaging properties of a hemispherical analyzer for nonrelativistic electrons. Knowledge of the trajectories and the associated imaging properties is essential for correctly specifying the analyzer parameters for optimum performance and for determining the energy resolution.

Figure 1 illustrates the parameters required for the analysis. The analyzer consists of concentric hemispheres having inner and outer radii r_2 and r_1, and

mean radius $r_0 = (r_1 + r_2)/2$. If we denote by $E_0 = \frac{1}{2} m v_0^2$ the kinetic energy of an electron that enters the analyzer at $\theta = 0$ and $r = r_0$ so that its trajectory is a circle of radius r_0, then the condition on the circular orbit requires that $mv_0^2/r_0 = e\kappa/r_0^2 = e\,|\mathbf{E}|$ where $\mathbf{E}$ is the radial electric field between the hemispheres and κ is a constant. This equation yields the electric field, $|\mathbf{E}(r)| = 2E_0 r_0/er^2$, the potential in the gap, $V(r) = (-2E_0 r_0/r) + c$ and the required voltage difference between the hemispheres, $\Delta V = E_0(r_2/r_1 - r_1/r_2)$.

From the equations of motion, $\ddot{r} - r\dot{\theta}^2 = -2r_0 E_0/mr^2$ and $dl/dt = mr^2\ddot{\theta} + 2mr\,\dot{r}\dot{\theta} = 0$ where $l = mr^2\,\dot{\theta}$ is the angular momentum, we obtain by the substitution $u = 1/r$ the equation of motion [13, 14]

$$\frac{d^2u}{d\theta^2} + u = \frac{2mr_0E_0}{l^2} \tag{1}$$

which has the solution

$$u = \frac{1}{r} = A_0 \cos\theta + B_0 \sin\theta + \frac{2mr_0E_0}{l^2} \tag{2}$$

where A_0 and B_0 are constants.

It is convenient to define the relative energy of the electron, $E \equiv E_0(1 + \eta)^2$, and $r = r_0(1 + \zeta)$ which specifies the trajectory radius of the electron relative to the mean radius r_0 at arbitrary points along the trajectory. In order to evaluate A_0 and B_0 in eqn. (2) l^2 must be expressed in terms of ζ and η. After the electron passes through the entrance slit, it is accelerated by the electric field $\mathbf{E}$. Taking into account the change in kinetic and potential energy as the electron crosses the entrance slit, one finds that $E^* = E_0[(1 + \eta^2) - 2\zeta_0/(1 + \zeta_0)]$ where $\zeta_0 = \zeta(\theta = 0)$ and E^* is the electron kinetic energy just inside the entrance slit (i.e., at $\theta = 0$). Using $E^* = \frac{1}{2} m((v_r^*)^2 + (v_\theta^*)^2)$ and $v_r^* = v_r = v_0(1 + \eta)\sin\alpha$ (i.e., the radial electron velocity is conserved as the particle crosses the entrance slit), the term on the right of eqn. (2) can be evaluated in terms of ζ_0, η and α

$$\frac{2mr_0E_0}{l^2} = \frac{1}{r_0}\left[(1 + \zeta_0)^2\left[(1 + \eta)^2\,(1 - \sin^2\alpha) - \frac{2\zeta_0}{1 + \zeta_0}\right]\right]^{-1} \tag{3}$$

The coefficients A_0 and B_0 can then be evaluated by application of the boundary conditions at $\theta = 0$ to yield a complete description of the electron trajectory between the hemispheres

$$r_0B_0 = \frac{\partial}{\partial\theta}\left(\frac{1}{1 + \zeta}\right)_{\theta=0} = \frac{-(1 + \eta)\sin\alpha}{1 + \zeta_0}\left[(1 + \eta)^2\,(1 - \sin^2\alpha) - \frac{2\zeta_0}{1 + \zeta_0}\right]^{-1/2} \tag{4}$$

$$r_0 A_0 = \frac{1}{1+\zeta_0} - \left[(1+\zeta_0)^2 \left[(1+\eta)^2\ (1-\sin^2\alpha) - \frac{2\zeta_0}{1+\zeta_0}\right]\right]^{-1} \tag{5}$$

where $\zeta_0 = \zeta(\theta = 0)$.

The imaging properties of the 180° spherical deflection analyzer can be obtained from eqn. (2) evaluated at $\theta = \pi$ and $\theta = 0$

$$\frac{1}{r_0(1+\zeta_\pi)} = -A_0 + \frac{2mr_0E_0}{l^2}\ (\theta = \pi) \tag{6}$$

$$\frac{1}{r_0(1+\zeta_0)} = A_0 + \frac{2mr_0E_0}{l^2}\ (\theta = 0) \tag{7}$$

After adding eqn. (6) and eqn. (7), substitution of eqn. (3) for the term containing l^2 and algebraic manipulation which makes use of the fact that $\Delta E = E - E_0 = \eta(\eta+2)E_0$ the final result is obtained

$$\zeta_\pi = -\zeta_0 - 2\left[1 - \frac{1}{1+\sin^2\alpha - \dfrac{\Delta E}{E_0}(1-\sin^2\alpha)}\right] \tag{8}$$

Equation (8) is an exact expression giving $\zeta(\theta = \pi) = \zeta_\pi$ as a function of $\zeta(\theta = 0) = \zeta_0$, the entrance angle α and the initial relative kinetic energy $\Delta E/E_0 = (E - E_0)/E_0$. For small $\Delta E/E_0$ and small α, eqn. (8) reduces to the approximate formula cited by others [15, 16]

$$\zeta_\pi = -\zeta_0 - 2\alpha^2 + \frac{2\Delta E}{E_0} \tag{9}$$

It is interesting to note that ζ_π in either eqn. (8) or (9) is independent of the sign of α, i.e., α appears only as a second order term. This is a result of the stigmatic focusing of the 180° deflection spherical analyzer.

Equation (8) provides the basis for determining the imaging properties of the hemispherical analyzer, and for optimizing its performance. In following sections, eqn. (8) is used to select entrance slit parameters, evaluate the energy window of a multichannel detection analyzer, establish criteria for determining energy resolution, and to optimize the analyzer étendue.

CHOICE OF ENTRANCE SLIT GEOMETRY

The entrance slit geometry of a multichannel detection analyzer can be chosen to simplify processing of signals the array detector. Figure 2 illustrates the plane of the analyzer which contains the entrance slit and exit plane at the array detector. The principal plane of the analyzer is represented

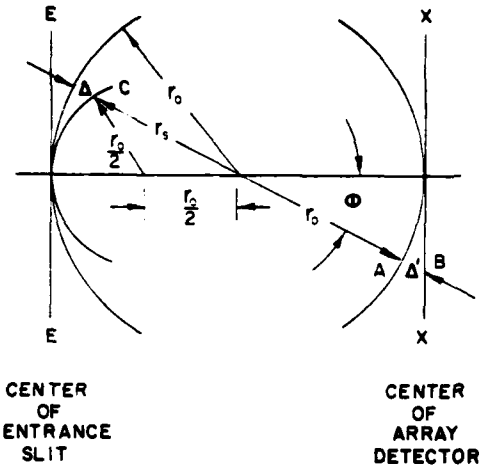

Fig. 2. Entrance and exit plane parameters required to describe the entrance slit shape (refer to text). Points A, B, and C lie on a line through the center. E—E (X—X) line through the center of the entrance slit (array detector) perpendicular to the central electron orbit. Point C lies on a line described by $r_s = r_0 (2 - \sec \theta)$ which is approximated by a circle of radius $r_0/2$.

by the horizontal line which intersects the centers of the entrance slit and the array detector. Vertical lines drawn a distance r_0 from the center represent the entrance slit center (E—E) and array detector center (X—X). Ideally, one would like to have identical rectangular-shaped energy channels for multichannel energy detection because, in this case, a single spatial parameter is sufficient to specify the energy of electrons which reach the detector. In Fig. 2, Δ' represents the radial distance from point A on the arc of radius r_0 to the point B on the line X—X through the center of the array detector. The distance between A and B is equal to $\Delta' = r_0 (\sec \phi - 1)$. According to eqn. (8), in order to arrive at point B an electron having energy E_0 must have originated from a point C in the entrance slit plane which is specified by the same angle ϕ and a radius equal to $r_s = r_0 - \Delta = r_0 (2 - \sec \phi)$.

The locus of points described by ϕ and $r_0 (2 - \sec \phi)$ is approximated for small ϕ by a circle of radius $r_0/2$ as shown in Fig. 2. This approximation is adequate for analyzing the slit geometry of a multichannel detector as long as points described by (r_s, ϕ) do not deviate from the arc corresponding to $r_0/2$ by an amount greater than 20% of the slit width $2a$. For $a/r_0 = 0.01$, this error is approximately equal to the slit width for $\phi = 20°$, but negligible for $\phi < 10°$.

This result shows that by choosing the entrance slit in the shape of an arc having radius $r_0/2$ (or, more precisely, according to $r_s(\phi)$) the energy channel bins at the exit plane can be made rectangular. The energy resolution depends on how the size and shape of the array of "rectangular" energy bins

at the exit plane are affected by the energy term ($\Delta E/E_0$) and angle terms ($\sin^2 \alpha$) in eqn. (8). In reality, even with a properly curved entrance slit, the "rectangular" energy bins are slightly curved for $E \neq E_0$, and the height of the image increases with r in the detector plane. However, within the constraints established in the next sections, one can assume that the energy dispersion is a linear function of a single geometrical parameter, the distance along the central plane. In other words, the detector will see n identical rectangular channels each representing the same increment in electron kinetic energy.

ENERGY WINDOW OF THE ANALYZER

We define the energy window of the analyzer as the energy range which can be simultaneously detected with linear energy dispersion in the focal plane. The exact energy window depends on the entrance slit width, $2a$, and α_{max}, the angular width of the beam which is allowed to enter the slit. In all cases of practical interest $\alpha^2 \ll 1$, therefore, the energy window can be accurately estimated using eqn. (8) assuming $\alpha^2 \cong 0$. Defining $r_{max} = r_1/r_0$ and $r_{min} = r_2/r_0$, the energy window relative to the pass energy E_0 is

$$\frac{E_{max} - E_{min}}{E_0} = \frac{r_{max} - 1}{r_{max} + 1} - \frac{r_{min} - 1}{r_{min} + 1} \tag{10}$$

or using $2r_0 = r_1 + r_2$, and $2 = r_{max} + r_{min}$

$$\frac{E_{max} - E_{min}}{E_0} = \frac{4(r_{max} - 1)}{(1 + r_{max})(3 - r_{max})} \tag{11}$$

The maximum energy window, equal to $\frac{4}{3}E_0$, occurs, as one would expect, when the largest gap is chosen ($r_{max} = 2$, $r_{min} = 0$). This is an impractical limit because as $r_{min} \to 0$, the gap voltage $\Delta V \to \infty$. In most cases of practical interest, various constraints including proper field termination and image detector size usually dictate designs having $r_2 \sim r_1/2$ (refer to later discussion and papers referenced in relation to this discussion). In this case the energy window is equal to approximately $\frac{1}{2}E_0$. An accurate determination of the energy window clearly requires taking into account the slit width and α, and should include analysis of the electron trajectories at E_{max} and E_{min} for suitable values of α to check that electrons having kinetic energies within the energy window do not collide with the inner or outer spheres. This procedure requires evaluation of eqn. 2 as a function of θ.

ENERGY RESOLUTION AND INTENSITY PROFILE

In order to determine the energy resolution, one must obtain the intensity

distribution at the plane of the image detector as a function of energy for specified entrance parameters including the entrance slit width, and the spatial and angular profile of the electron beam at the entrance slit. Similar analyses for a semicircular magnetic analyzer [15, 16], and electrostatic analyzers based on 127° cylindrical [17] and 180° hemispherical [18] capacitors have been reported. However, none of these treatments consider how overlap of the intensity distribution profiles affects the conditions for optimizing energy resolution and luminosity of a spherical capacitor analyzer. In most cases, assuming a uniform intensity over the entrance slit area and over the angle is adequate for determining the performance of an analyzer. In general, this will represent a worst case for studying energy resolution because more realistic assumptions usually involve spatial and angular distributions peaked near the center of the slit and at entrance angles near $\alpha = 0$.

For the purpose of evaluating the intensity profile at the exit plane using eqn. (8), it is convenient to rewrite eqn. (8) by defining the following parameters: $x = r - r_0$, $\epsilon = (E - E_0)/E_0$. We will show later that proper design requires $\alpha^2 \leqslant a/2r_0$, and that, in practical cases, $a/2r_0 \ll 1$. With these constraints and the parameters defined above, eqn. (8) becomes

$$x_2 \cong -x_1 - 2r_0 + \frac{2r_0}{(1-\epsilon)\left(1 + \alpha^2\left(\frac{1+\epsilon}{1-\epsilon}\right)\right)} \tag{12a}$$

or

$$x_2 \cong -x_1 + 2r_0\left(\frac{\epsilon}{1-\epsilon}\right) - 2r_0\,\alpha^2\left(\frac{1+\epsilon}{(1-\epsilon)^2}\right) \tag{12b}$$

Based on the assumption of uniform electron flux distribution at the entrance slit over space and angle, the intensity distribution at the exit plane can be evaluated analytically using eqn. (12). Positive and negative angles contribute equally to the intensity at any given point on the detector (for a given E) so that the intensity at point x_2 is given by

$$I(x_2) = 2\int I(x_2, \alpha)\,\mathrm{d}\alpha = 2k\int \mathrm{d}\alpha \tag{13}$$

where $I(x_2, \alpha)$ is the intensity at x_2 for a given α at the entrance slit, and k is a proportionality constant.

Let us consider the range of x_2 corresponding to a given energy, E, a given entrance slit width, $2a$, and a given maximum angle, α_m. (The continuous interval for the variable x_2 at a given energy E arises because the angle α may take any value between $-\alpha_m$ and $+\alpha_m$ in our model.) Using eqn. (12b) and defining

$$\Sigma = \frac{(1+\epsilon)}{(1-\epsilon)^2} \tag{14a}$$

$$\phi = 2r_0 \alpha^2 \Sigma \tag{14b}$$

$$\psi = 2r_0 \frac{\epsilon}{1-\epsilon} \tag{14c}$$

we can show that the maximum and minimum values of x_2 as a function of ϵ, a and α_m are given by

$$x_{2\max} = a - 2r_0 + \frac{2r_0}{1-\epsilon} \tag{15a}$$

$$x_{2\min} = -a - 2r_0 + \frac{2r_0}{1+\alpha_m^2 - \epsilon(1-\alpha_m^2)} \tag{15b}$$

where $x_1 = -a$ (a) and $\alpha^2 = 0$ $(\alpha_{\max}^2)$ for $x_{2\max}$ $(x_{2\min})$. Therefore, the width of the intensity distribution at its base is given by

$$x_{2\max} - x_{2\min} = 2a + \frac{2\alpha_m^2(1+\epsilon)r_0}{(1-\epsilon)(1+\alpha_m^2 - \epsilon(1-\alpha_m^2))} \tag{16a}$$

or since $\alpha_{\max}^2 \ll 1$

$$x_{2\max} - x_{2\min} \cong 2a + 2r_0 \alpha_m^2 \Sigma \tag{16b}$$

The shape of the intensity distribution is obtained by evaluating eqn. (13). From eqn. (14), we have

$$\phi = -x_2 - x_1 + \psi \tag{17a}$$

$$\phi_{\max} = -x_2 + a + \psi \tag{17b}$$

$$\phi_{\min} = -x_2 - a + \psi \tag{17c}$$

and in addition, ϕ satisfies the conditions: $\phi \geqslant 0$, $\phi \leqslant 2r_0 \alpha_m^2 \Sigma$ and $\phi_{\min} \leqslant \phi \leqslant \phi_{\max}$. These conditions determine the range of integration for evaluating eqn. (13). The range is illustrated in Fig. 3. The special points labeled e, f, g and h along the x_2 axis of Fig. 3 are given by

$$e = \psi - a(1+\Sigma) \tag{18a}$$

$$f = \psi + a(1-\Sigma) \tag{18b}$$

$$g = \psi - a \tag{18c}$$

$$h = \psi + a \tag{18d}$$

and the limits of integration over α corresponding to the three shaded areas in Fig. 3. are given by

$$\mu = \sqrt{\frac{a}{2r_0}} \tag{19a}$$

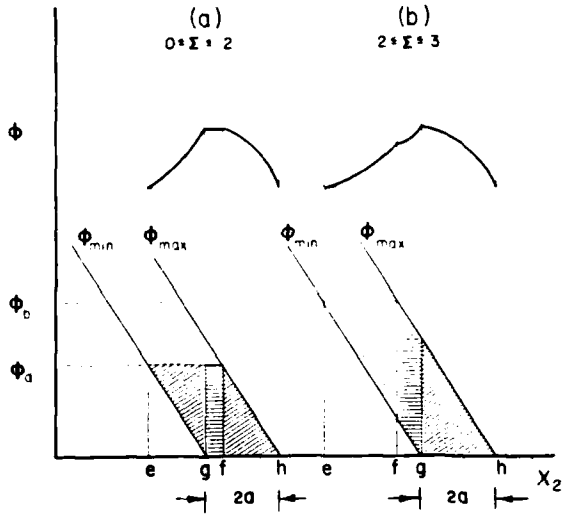

Fig. 3. Illustration of the range of angles which contribute to the integration over α to determine intensity profiles (refer to text). Panels (a) and (b) correspond to two cases when g < f and g > f. Upper figures illustrate the intensity profiles.

$$\nu = \sqrt{\frac{\psi - a - x_2}{2r_0\Sigma}} \tag{19b}$$

$$\omega = \sqrt{\frac{\psi + a - x_2}{2r_0\Sigma}} \tag{19c}$$

Equations (19a–c) are based on the choice $\alpha_m^2 = a/2r_0$ which we will show later optimizes the étendue. The intensity distribution at the detector in the two cases $0 < \Sigma < 2$ and $2 < \Sigma < 3$ are

$0 < \Sigma < 2$	x_2 in [e,g]	$I = 2k(\mu - \nu)$	(20a)
or $-1 \leqslant \epsilon \leqslant \frac{1}{3}$	x_2 in [g,f]	$I = 2k\mu$	(20b)
	x_2 in [f,h]	$I = 2k\omega$	(20c)
$2 \leqslant \Sigma \leqslant 3$	x_2 in [e,f]	$I = 2k(\mu - \nu)$	(21a)
or $\frac{1}{3} \leqslant \epsilon \leqslant \frac{1}{3}$	x_2 in [f,g]	$I = 2k(\omega - \nu)$	(21b)
	x_2 in [g,h]	$I = 2k\omega$	(21c)

These intensity distributions are plotted in Fig. 3 (above the graph of ϕ) and illustrate how the shape of the image depends on ϵ for a uniformly illuminated entrance slit.

We now consider the energy resolution. Referring back to eqn. (16), and to the intensity distributions illustrated in Fig. 4, one can define, operationally,

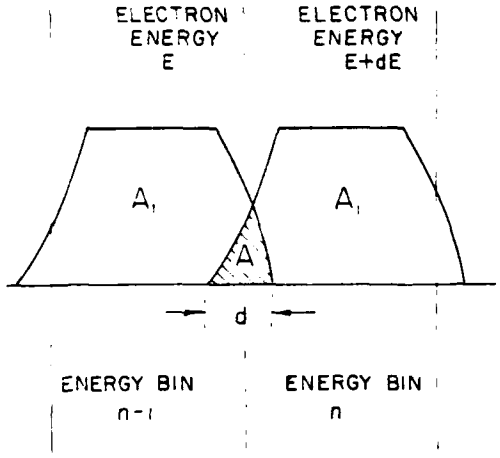

Fig. 4. Intensity profiles for electrons having energy E and $E + dE$ superimposed on two detector energy bins. The energy resolution is defined in terms of the overlap between adjacent intensity distribution.

the energy resolution in terms of the overlap of two adjacent intensity distributions corresponding to energies E and $E + dE$. High energy resolution results from suitably small overlap of the intensity distributions corresponding to adjacent energies. Note that we are careful to distinguish between the intensity distributions which are a property of the imaging characteristics of the analyzer, and the energy bins which are determined by how the detector electronics processes the image. We choose to characterize the overlap of intensity distributions by two parameters: d, which represents the baseline overlap of the intensity distributions corresponding to adjacent energy channels which we wish to resolve, and F, which represent the fractional area of overlap of adjacent intensity distribution profiles $F = A/(A + A_1)$ Fig. 4). Clearly, high energy resolution will be associated with a suitably small F, and a value of d which is a small fraction of $x_{2\max} - x_{2\min}$ for a given energy. We define the distance d in terms of the baseline width and a parameter γ by $(x_{2\max} - x_{2\min})/\gamma = d$.

The relative energy resolution, δe, can now be expressed in terms of the analyzer parameters by requiring that δe (or equivalently d) be chosen to achieve a desired low value of F (i.e., 1/10). We require $x_{2\min}(\epsilon + \delta e) = x_{2\max}(\epsilon) - d$ (Fig. 4). Using eqns. (15) and (16b) this requirement becomes

$$\frac{2}{1 + \alpha_m^2 - (\epsilon + \delta e)(1 - \alpha_m^2)} - \frac{2}{1 - \epsilon} = \frac{-2\alpha_m^2}{\gamma}\Sigma + \frac{2a}{r_0}\left(\frac{\gamma - 1}{\gamma}\right) \qquad (22)$$

or

$$\delta e = (1+\alpha_m^2)/(1-\alpha_m^2) - \epsilon - \frac{1}{(1-\alpha_m^2)\left\{\frac{1}{1-\epsilon} - \frac{\alpha_m^2}{\gamma}\Sigma + \frac{2a}{r_0}((\gamma-1)/2\gamma)\right\}} \tag{23}$$

Equation (23) can be expanded in α_m^2 ($2a/r_0$ being of the order of α_m^2) to yield

$$\delta e = (1-\epsilon)^2 \frac{2a}{r_0}\left(\frac{\gamma-1}{2\gamma}\right) + \alpha_m^2\left[1+\epsilon-\frac{1+\epsilon}{\gamma}\right] \tag{24}$$

By computing $\partial(\delta e)/\partial(\epsilon)$ from eqn. 24, and noting that it is very small (because $2a/r_0 \approx \alpha_m^2$), δe can be regarded as being constant with respect to ϵ, and we can assume $\epsilon = 0$. In this case, δe reduces to

$$\delta e \approx \left(\frac{2a}{r_0} + 2\alpha_m^2\right)\left(\frac{\gamma-1}{2\gamma}\right) \tag{25}$$

This expression will be used later to maximize the étendue of the analyzer. First, we determine the value of γ which yields an overlap ratio F of less than 10%. The area under adjacent intensity distribution curves can be found by integration using the functional dependence of the curves given in eqn. (20) (for $0 < \Sigma < 2$) and eqn. (21) (for $2 \leqslant \Sigma \leqslant 3$).

$$0 \leqslant \Sigma \leqslant \frac{2}{2\gamma-1}$$

$$F = \frac{2-(\gamma-1)\Sigma}{2\gamma} \tag{26a}$$

$$\frac{2}{2\gamma-1} \leqslant \Sigma \leqslant 3$$

$$F = \frac{\Sigma}{6} - \frac{[(2\gamma-1)\Sigma-2]^2}{8\gamma^2\Sigma} + \frac{[(2\gamma-1)\Sigma-2]^3}{24\gamma^3\Sigma^2} + \frac{1}{3\sqrt{\Sigma}} \times \left[\frac{[2\gamma-1)\Sigma-2]^2}{4\gamma^2\Sigma} + \frac{2}{\gamma} - \frac{\gamma-1}{\gamma}\Sigma\right]^{3/2} \tag{26b}$$

Considering the worst case ($\Sigma = 0$ which corresponds to rectangular intensity distributions) an estimate of γ based on the requirement that $F \approx \frac{1}{10}$ is $\gamma = 10$. Table 1 illustrates the relationship between the relative areas as a function of Σ for various values of γ.

In the next section, we will show that the maximum étendue occurs when

TABLE 1

$F \times 100$ REPRESENTING THE OVERLAP RATIO $A/(A + A_1)$ (EXPRESSED AS A PERCENTAGE) FOR DIFFERENT VALUES OF BOTH THE PARAMETER γ AND THE ENERGY-DEPENDENT VARIABLE Σ. THE TABLE SHOWS CLEARLY THAT FOR $\gamma = 10$ THE AREA A IS ALWAYS LESS THAN 10% OF $(A + A_1)$

Σ	$\gamma = 4$	$\gamma = 6$	$\gamma = 8$	$\gamma = 10$
0.000	25.00	16.66	12.50	10.00
0.050	23.12	14.58	10.31	7.75
0.105	21.06	12.29	7.91	5.27
0.133	20.00	11.11	6.67	4.27
0.182	18.18	9.09	5.11	3.27
0.586	8.92	3.96	2.23	1.43
1.000	7.03	3.13	1.76	1.13
1.500	6.38	2.84	1.60	1.02
2.000	6.25	2.78	1.56	1.00
2.500	6.33	2.81	1.58	1.01
3.000	6.51	2.89	1.63	1.04

one chooses $\alpha_m^2 = a/2r_0$. Using this value for α_m^2 and $\gamma = 10$, eqn. (25) yields

$$\delta e \approx \left[\frac{2a}{r_0} + \frac{a}{r_0}\right]\left[\frac{\gamma - 1}{2\gamma}\right] \approx \frac{27}{20}\frac{a}{r_0} \tag{27}$$

THE ANALYZER ÉTENDUE

The performance (resolution and intensity) of a hemispherical analyzer with fixed entrance and exit slits and a specified pass energy E_0 is determined by the entrance slit parameters (i.e., the maximum aperture angle α_m and relative slit width $a/2r_0$) and by the relative width of the exit slit $b/2r_0$. One of the most important considerations in analyzer design, whether the analyzer is to utilize single channel (an exit slit) or multichannel (an array detector) detection is that of maximizing the luminosity (product of étendue and transmission). The étendue of the energy dispersive part of an energy analyzer is the product of entrance slit area x entrance solid angle, and the transmission is the ratio of flux which leaves the exit slit to the flux which enters the entrance slit at a given energy. It is important to note that the étendue, as defined above, does not necessarily apply to the entire analyzer including input optics, but can be translated through the input optics to represent a figure of merit for the entire spectrometer at any particular retardation ratio provided the properties of the input lens system are accurately known.

The étendue can be expressed (Fig. 1) as $E' = 4\alpha_m \beta_m ah$, (where β is defined in Fig. 1, and the subscript m designates the maximum allowed value). From eqn. (9), the energy resolution of the spherical analyzer with fixed slits (based on the FWHM [18, 19] can be written $R = 2r_0/(a + b + 2\alpha_m^2 r_0)$ where α_m^2 is the maximum value of α^2. The parameters β_m and h do not enter into E' in relation to the energy resolution, $\Delta E/E_0$, and the maximum value of E' for a specific $\Delta E/E_0$ depends only on the choice of α_m and a. With the assumption $a = b$, $dE'/d\alpha_m = 0$ yields $\alpha_m^2 = a/2r_0$. A more detailed analysis which takes into account the transmission function of the analyzer can be performed [18]. The calculation requires knowledge of the slit illumination. If uniform illumination is assumed ($dI/d\zeta_0 = \text{const.}$, $dI/d\alpha = \text{const.}$) an exact analytical expression can be obtained for α_m^2: $\alpha_m^2 = \frac{4}{5}(a/2r_0)$. Clearly, in fixed slit analyzers where $a \simeq b$, it is best to choose $\alpha_m^2 \simeq a/2r_0$.

Equation (25), which describes the relative energy resolution of a multichannel detection analyzer in terms of the relevant parameters may be used to determine the condition for maximum étendue at constant energy resolution when parallel energy detection is incorporated. Solving eqn. (25) for a and substituting into the expression for the étendue, $E' = 4\alpha_m \beta_m ah$, one obtains

$$E' = \frac{2\beta_m h}{p}(e - q\alpha_m^2)\alpha_m \tag{28}$$

where $p = (\gamma - 1)/2\gamma r_0$ and $q = (\gamma - 1)/\gamma$. The étendue is maximized by $(\partial E'/\partial \alpha_m) = e - 3q\alpha_m^2 = 0$ or $3q\alpha_m^2 = q\alpha_m^2 + 2pa$. This leads to the condition $\alpha_m^2 = (pa/q) = (a/2r_0)$ which is the same result as that obtained by simple analysis of an analyzer with fixed entrance and exit slits, assuming equal slit widths. This result is not obvious, but does not contradict one's intuition. The same general condition was used to constrain both cases, i.e., to maximize the étendue.

NUMBER OF CHANNELS AND PRACTICAL DESIGN CONSIDERATIONS

The theoretical number of energy channels that can be achieved is equal to the total energy window divided by the energy resolution. In the section headed "Energy window of the analyzer", we have shown that the maximum energy window is $\frac{4}{3}E_0$, but practical limitations restrict this to values of approximately $\frac{1}{3}E_0$. With $\alpha_m^2 = \alpha/2r_0$, the relative energy resolution based on our criteria for overlapping intensity distributions is $\delta e = (\delta E/E_0) = \frac{27}{20}(a/r_0)$ which yields a number of energy channels equal to

$$n = \frac{\frac{1}{3}E_0}{\frac{27}{20}\left(\frac{a}{r_0}\right)E_0} \cong \frac{r_0}{4a} \tag{29}$$

We can now make some informed comments regarding how the source size, the size and spatial resolution of the imaging detector, and the required energy resolution affect the choice of the analyzer parameters r_0 and $2a$ using a specific example.

We consider the design of an angle resolving electron analyzer which is intended to be used in off-specular scattering vibrational spectroscopy. The required energy resolution is 5 meV and because the intensity of signals detected in off-specular scattering is extremely low, one would like to achieve the greatest number of energy channels possible. Since the counting rate is expected to be very low, and a large number of channels are desired, a commercial array detector which achieves 100 line pair resolution over a 2.5 cm diameter surface at counting rates approaching 10^5 Hz is a good choice. In cases where much higher counting rates are expected, individual anodes with individual high speed amplifiers or optically coupled devices would represent more appropriate choices.

The first question which must be addressed is the size of the analyzer, i.e., the selection of the mean radius r_0. The most important factor in choosing r_0 is the source size because the source size, the required energy resolution and the energy range (i.e., the retardation required in the input lens system) will constrain the size of the entrance slit. Multichannel detection does not make sense if reasonable efforts have not been made to optimize analyzer performance taking into account other important factors including size limitations. We have chosen an example in which many years of development by a number of groups has led to a reasonably well optimized design for single channel instruments. This existing design serves as a very good starting point for a multichannel design.

Specifically, current vibrational spectrometers utilize an entrance slit width of a few tenths of a millimeter to achieve 5 meV energy resolution over energy ranges extending to 300 eV. These designs are fairly well optimized to a source consisting of an electron microscope filament, and we assume that the multichannel instrument being considered here will utilize a similar source. With an entrance slit width of 0.25 mm, and a 2.5 cm diameter image detector having spatial resolution of 100 line pairs per 2.5 cm, one can reasonably expect to achieve 50—100 energy channels provided proper entrance slit conditions are maintained ($\alpha^2 < a/2r_0$), and that stray fields and other technical considerations discussed in the following section are properly taken into account. With a slit width of 0.25 mm, and an energy resolution of 5 meV, an analyzer having $r_0 = 10$ cm would operate at 3 eV pass energy. The 10 cm radii and 2 eV pass energies are larger (by about a factor of 3) than corresponding parameters for single channel vibrational instruments, however, the larger r_0 is necessary to comfortably achieve a 2.5 cm gap required for the commercial image detector.

Technical considerations

In order to achieve optimum performance of an energy analyzer, one must ensure that stray fields do not affect the electron trajectories. Obvious precautions must be taken to shield electrical leads, which provide lens voltages, and insulators which may support surface charge and thus produce electric fields. Magnetic fields can have a major effect on electron trajectories in analyzers operating at low pass energies. Assuming a constant magnetic field perpendicular to the circular electron orbits, one can show that the ratio of electric to magnetic forces in a hemispherical analyzer is given by $(F_m/F_e)^2 = (e^2 r_0^2 B^2/2mE_0)$. In an analyzer with $r_0 = 10$ cm and operating at a 1 eV pass energy, B must be less than 1 mG for electron detection if changes introduced in the trajectories are to be less than a few percent of r_0 at the detector plane.

A more elaborate analysis [20] which includes the effect on the shape and position of the intensity distribution curve can be performed by including the magnetic field in the equation of motion. In this case, we define two energies (relative to E_0) E'/E_0 and E''/E_0 corresponding to $\bar{\zeta}_2'$ and $\bar{\zeta}_2'$ (ζ_2' and ζ_2'') defined as the corresponding positions at the exit plane when a magnetic field is present (absent). Calculations of the electron trajectories for $E_0 = 0.5$ eV (representing a low energy estimate of the analyzer described in the previous section) and assuming the worst case direction of magnetic field (B perpendicular to the orbit), we have shown that

$$\Delta_B = \frac{(\zeta_2' - \bar{\zeta}_2') - (\zeta_2'' - \bar{\zeta}_2'')}{\zeta_2' - \zeta_2''} < \frac{1}{100}$$

for B less than 1 mG and for any E' and E'' such that $E' - E'' \geqslant 1$ meV. The parameter Δ_B may be regarded as a parameter which characterizes the degree of distortion of the image (as a function of position ζ_2') when a magnetic field is present. If $\Delta_B = 0$ for all ζ_2' corresponding to the entire energy range, then the effect of the magnetic field is merely to shift the intensity distribution by an amount equal to $\zeta_2' - \zeta_2'' = \bar{\zeta}_2' - \bar{\zeta}_2''$. For $B_z = 1$ mG and $E_0 = 0.5$ eV, we have shown that $\zeta_1' - \zeta_2''$ is 0.3–0.5 mm (which is of the order of the entrance slit dimension 0.35 mm), but that $\Delta_B < 0.01$. The effect of other magnetic field directions is even less [20], and the magnetic perturbations decrease as the pass energy is increased. In general, the effects of low (milliGauss) level magnetic fields can be taken into account by an accurate energy calibration of the analyzer (using gas phase photoemission, for example) at a given pass energy.

One of the most difficult problems to solve in a multichannel detector electron energy analyzer is that of field terminations at the entrance slit and the detector. The entrance slit problem has been treated for 180° spherical analyzers in detail by several authors [21–23] and can be solved adequately using careful slit design. Field termination at the array detector

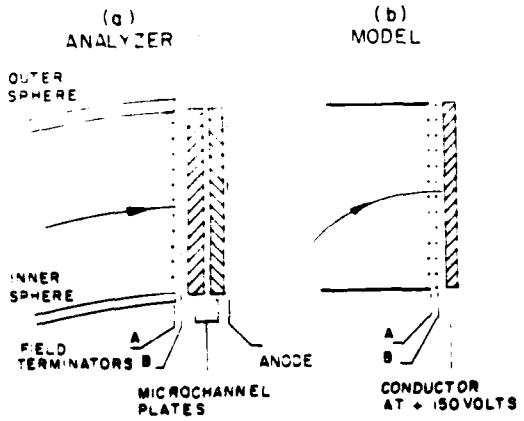

Fig. 5. (a) Cross section of spherical analyzer at the array detector showing electric field terminators. (b) Two dimensional model of the terminator used in electron ray tracing analysis of electric fields and electron trajectories for various field termination configurations. Terminator A consists of individual metal ribbons biased to duplicate the $1/r$ potential. Terminator B is a high transmission wire mesh.

presents a more difficult problem which has been treated in some detail by others [8, 24]. Figure 5 illustrates a cross sectional view of a hemispherical analyzer at the array detector and the model we have used to investigate the properties of several field termination configurations. Efficient detection by a channel plate electron multiplier requires electrons to impact the channel plate surface at kinetic energies of about 100 eV. An analyzer operating at low pass energies (~ 1 eV) therefore requires a 100 eV accelerating potential between the sphere voltages and the first channel plate. Without suitable field terminations, the perturbation to the $1/r$ field would be severe.

We have used electron ray tracing techniques to investigate several field termination configurations (as well as input lens designs [25—27] and have found a configuration which should yield over 80% transmission and which provides adequate termination of a 100 eV potential to permit multichannel detection at 1 eV pass energies. We have found, empirically, by studying the perturbation in trajectories of 1 eV electrons, that at least two termination grids are required. A double grid, as shown in Fig. 5, consisting of 30 equidistant 1×20 mm ribbons (95% transmission) biased to produce the $1/r$ potential followed by a fine wire (90% transmission) mesh maintained at the potential equal to that at r_0 produces an adequate termination [20]. A similar termination has been reported to work well at $E_0 = 2$ eV by another group [8].

ACKNOWLEDGMENT

This work was sponsored by the National Science Foundation Grant DMR 8304368.

REFERENCES

1 M. Lamption and C.W. Carlson, Rev. Sci. Instrum., 50 (1979) 1093.
2 C. Firmani, E. Ruiz, C.W. Carlson, M. Lampton and F. Paresee, Rev. Sci. Instrum., 53 (1982) 570.
3 L. Mertz, T.D. Tarbell and A. Title, Appl. Opt., 21 (1982) 628.
4 D. Rees, I. McWhirter, P.A. Rounce, F.E. Barlow and S.K. Kellock, J. Phys. E, 13 (1980) 763.
5 D. Rees, I. McWhirter, P.A. Rounce, and E.E. Barlow, J. Phys. E, 14 (1981) 229.
6 Surface Science Laboratories Inc., Palo Alto, CA.
7 P.C. Stair, Rev. Sci. Instrum., 51 (1981) 132.
8 J.E. Pollard, D.J. Trevor, Y.T. Lee and D.A. Shirley, Rev. Sci. Instrum., 52 (1981) 1837.
9 P.J. Hicks, S. Daviel, B. Wallbank and J. Comer, J. Phys. E, 13 (1980) 713.
10 W. Aberth, Int. J. Mass Spectrom. Ion Phys., 37 (1981) 379.
11 R.W. Odom, B.K. Furman, C.A. Evans, C.E. Bryson, W.A. Petersen and M.A. Kelly, Anal. Chem., in press.
12 D.W.O. Heddle, J. Phys. E, 4 (1971) 589.
13 E.M. Purcell, Phys. Rev., 15 (1938) 818.
14 S.W. McCuskey, An Introduction to Advanced Dynamics, Addison-Wesley, Reading, MA,. 1959, see in particular Chap. 3 and Problem 3.3.
15 K. Siegbahn, α, β and γ Ray Spectroscopy, North-Holland, 1955, Chap. 3.
16 C.S. Fadley, R.N. Healey, J.M. Hollander and C.E. Miner, J. Appl. Phys., 43 (1972) 1085.
17 H. Froitzheim, J. Electron Spectrosc. Relat. Phenom., 34 (1984) 11.
18 H.D. Polaschegg, Appl. Phys., 9 (1976) 223.
19 C.E. Kuyatt and J.A. Simpson, Rev. Sci. Instrum., 38 (1967) 103.
20 A comprehensive analysis of the effects of magnetic fields on electron trajectories in a spherical analyzer is available in F. Hadjarab, Masters Degree Thesis, University of Texas at Austin, 1984.
21 K. Jost, J. Phys. E, 12 (1979) 1001.
22 R. Herzog, Z. Phys., 97 (1935) 596; 41 (1940) 18.
23 D. Roy and J.D. Carette, in H. Ibach (Ed.), Topics in Current Phys., Vol 4, Springer, Berlin, 1977, pp. 13—58.
24 C. Oshima, R. Franchy and H. Ibach, Rev. Sci. Instrum., 54 (1983) 1042.
25 Our electron ray tracing studies utilized the electron trajectory program SLERT developed by W.B. Herrmannsfeldt at the Stanford Linear Accelerator (SLAC Report No. 226). Details of the program are contained in refs. 26 and 27.
26 G.K. Ovrebo and J.L. Erskine, J. Electron Spectrosc. Relat. Phenom., 24 (1981) 189.
27 H.A. Stevens, A.W. Donoho, A.M. Turner and J.L. Erskine, J. Electron Spectrosc. Relat. Phenom., 32 (1983) 327.

Journal of Electron Spectroscopy and Related Phenomena, 39 (1986) 265–272
Elsevier Science Publishers B.V., Amsterdam – Printed in The Netherlands

ADVANCED ELECTRON OPTICS FOR VIBRATIONAL SPECTROSCOPY

J. L. Erskine
Department of Physics, University of Texas, Austin Texas 78712

ABSTRACT

Requirements for a "next generation" high resolution electron energy loss spectrometer for probing surface vibrations are proposed based on several specific applications in which the performance of present generation instruments is marginal or totally inadequate. Prospects of achieving significant improvements are explored and found to be very good for applications which involve studies of impact scattering phenomena. Results of zoom lens ray tracing studies, analysis of electron trajectories and exit plane images in a hemispherical analyzer in relation to multichannel energy detection and studies of electron trajectories near various field terminators are presented. A prototype analyzer / monochromator design is described which will be used to test the model calculations and to extend the applications of EELS to more detailed studies of impact scattering.

INTRODUCTION

High resolution electron energy loss spectroscopy (EELS) is now well established as one of the most useful probes of the physical and chemical properties of surfaces. The origin of the EELS technique can be traced back to the pioneering work reported by Propst and Piper in 1967 which demonstrated the feasibility of observing vibrational losses at surfaces using inelastic electron scattering (ref. 1). However, the development and practical applications of the technique experienced the most rapid growth after the introduction of refinements in EELS spectrometers by Ibach in 1970 (ref. 2) and by others (ref. 3). These improvements made possible routine high resolution (better than 10 meV) measurements of surface vibrations.

Significant additional progress has been achieved in improving the performance of EELS instruments since these early studies. Energy resolution of some new instruments has exceeded 3 meV FWHM (ref. 4), and the energy range over which surface vibrational losses can be probed at high resolution has been extended to over 300 eV making possible measurements of surface phonon bands throughout the entire two-dimensional Brillouin zone (refs. 5,6). The counting rates at which loss spectra are recorded have also been significantly improved. Instruments utilizing larger energy dispersing elements and incorporating more efficient coupling between the premonochromator and main monochromator (ref. 4) have achieved nearly an order of magnitude improvement of intensity compared with most existing instruments.

In spite of these improvements, the fact remains that nearly all of the "working" EELS instruments presently being used to study surface vibrations are based of the same fundamental design introduced over fifteen years ago. A few notable exceptions have recently appeared: Franchy and Ibach (ref. 7) have reported results obtained using a 127° EELS analyzer which utilizes a multichannel detection system. Ho (ref. 8) has reported studies of surface chemical dynamics using a similar instrument based on a 180° hemispherical analyzer, and Kevan and Dubois (ref. 9) recently described a new type of EELS optics based on dispersion compensation.

0368-2048/86/$03.50

Recent experimental and theoretical results in the area of surface vibrations have now demonstrated that the field is ripe for another rapid period of growth that could be stimulated by additional technical advances and improvements in instrumentation. Several calculations for surface phonons at semiconductor surfaces (refs. 10,11) have established a relationship between surface reconstruction of Si surfaces and the dispersion of surface phonon bands. Lattice dynamical analysis of adsorbate phonon bands (refs. 12-14) has been successfully used to obtain the height of oxygen on Ni(100). Calculations of the inelastic scattering cross section for adsorbates, in particular H on W(100), have also shown that the energy dependence of this parameter contains structural information (ref.15). Existing EELS instruments are capable of measuring phonon band dispersion (refs.12-14,16,17) and energy dependencies of impact scattering cross sections (refs. 17-19), but the measurements are fairly tedious due to low counting rates and technical difficulties related to sweeping the kinetic energy while probing a specific loss energy. Measured EELS cross sections are in general only approximate due to imprecise knowledge of the transmission function of the electron optics. Other exciting experiments such as time resolved experiments and studies of vibrational losses on technical surfaces having low adsorbate surface concentrations (as might be found on a model supported catalyst) are even more difficult or impossible to perform with existing spectrometers. Directed efforts to improve spectrometer performance are clearly justified for several of these new applications.

NEXT GENERATION EELS SPECTROMETERS

Specific configurations of next generation EELS spectrometers have not yet been established, but several characteristics of the most probable designs are becoming clear. For example, a single design is unlikely to provide optimum performance for all intended applications. Time resolved specular scattering experiments which probe dynamics of chemical processes at single crystal surfaces will require different instrument parameter optimization than studies which map surface phonons and measure angle and energy dependent cross sections. However, common elements of electron optics will be involved in all of the new designs. These elements include a more thorough understanding of lens systems, imaging properties of dispersive elements, the effects of fringing fields on electron trajectories near slits and image detectors, and high density charge transport in electron optical systems.

The purpose of this paper is to describe some of our recent work aimed at evaluating several of these factors with the goal of developing improved electron optics for a specific application. Based on our experience and continued interest in utilizing the EELS technique to probe surface phonon bands and scattering cross sections, we have proposed and are currently evaluating a new instrument for this application. Our general approach is based on constructing a prototype analyzer / monochromator based on these studies which is versatile enough to permit careful evaluation of various predictions related to electron optics performance.

REQUIREMENTS FOR IMPACT SCATTERING STUDIES

Accurate measurements of scattering cross sections require control of apertures in both the monochromator and analyzer to define the solid angles and sample area where scattering occurs

as well as careful characterization of the transmission properties of the spectrometer. The interesting energy range covers a few eV to several hundred eV. Phonon band mapping also requires good angle-defining apertures, to limit the range of $k_{||}$ probed in the Brillouin zone, as well as electron impact energies of several hundred eV. These two applications of EELS have similar requirements, therefore, a single instrument optimized for impact scattering studies and which achieves well defined angular acceptance will serve both applications. Inelastic electron losses measured in nonspecular scattering geometry rely on the impact scattering mechanism (ref. 8) which produces signal levels approximately two orders of magnitude below typical dipole loss signals. Clearly, high monochromator currents and more efficient detection while maintaining good energy resolution and low background counting rates are also of prime importance.

ENERGY ANALYZER

Figure 1 illustrates the general features of the new analyzer we have constructed which meets our requirements for higher detection efficiency, more precise control of solid angles and transmission properties and a broad impact energy range. The analyzer consists of hemispherical dispersing elements and a multichannel detection system coupled to tandem four-element zoom lenses. The monochromator consists of an identical set of lenses, apertures and hemispheres, and a premonochromator coupled to the entrance slit via a three-element zoom lens.

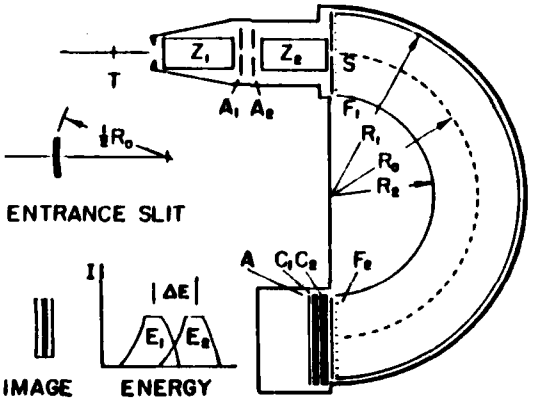

Figure 1: New parallel detection electron energy analyzer. Z_1 and Z_2 are four-element zoom lenses; A_1 and A_2 are angle-defining apertures; S is the entrance slit; R_1, R_2, and R_0 are the outer sphere, inner sphere and mean radius, respectively. The array detector consists of a resistive anode A, two channel plate electron multipliers C_1 and C_2, and a specially designed field terminator F_2. Insets illustrate the entrance slit shape required to yield rectangular exit plane images. Also illustrated is the spatial distribution of two adjacent energy channels when proper conditions are satisfied at the entrance slit.

Several factors were considered in arriving at this design configuration and considerable analysis of key features of the analyzer has been carried out. These results are described below and represent the major conclusions reported in this paper.

a. **Hemispheres:** Most existing EELS instruments are based on 127° cylindrical dispersive elements. However, the two dimensional imaging properties of a hemispherical analyzer should yield performance equal to or better than 127° sector based instruments having a comparable mean radius. Demuth and Avery (ref. 20) have achieved EELS instrument performance using hemispherical analyzer / monochromator designs which is comparable to the best performance of 127° cylinder instruments having similar mean radii. We have carried out a comprehensive analysis (ref. 21) of the image properties of the hemispherical analyzer in relation to applications involving multichannel energy detection. This work established criteria for optimizing detection efficiency, choosing entrance slit parameters and the number of channels. Our analysis of the imaging properties of hemispherical analyzers has shown that the same entrance slit conditions necessary to achieve optimum resolution and transmission in a single channel real slit analyzer also yield optimum flux and images properties at the exit plane required for multi channel detection. For an EELS spectrometer based on a conventional hot cathode source (which defines the fundamental size parameter of the instrument), achieving 50 energy channels at ~10meV resolution is not an unreasonable expectation. The spatial resolution of commercially available image detectors based on resistive anodes now exceeds 100 line pairs per inch, and the maximum counting rate that can be achieved by these detectors are within the range expected in applications based on impact scattering.

b. **Mean Radius:** Practical considerations (ref. 21) require that the hemispheres provide a gap of about one inch and a mean radius, r_o, of the order of 2.5 inches to accommodate an array detector. This value of r_o is considerably larger than that of most existing EELS analyzers and presents some difficulties (i.e., a larger vacuum chamber, higher costs for magnetic shielding) but also offers several advantages. One advantage is that high resolution can be achieved using larger slit dimensions and higher pass energies. Higher pass energies permit smaller retardation / acceleration ratios in the lens systems. This reduces undesired effects on electron trajectories within the hemispheres due to inhomogeneity of the surface potentials. Larger slits also provide the possibility of better coupling to the source. All of these factors can contribute to better performance, and probably account for the fact that some of the newer instruments which have achieved the best performance use large mean radii in the analyzer and main monochromator.

c. **Lens System:** It is well known that aberrations limit the image quality in electron lens systems. In the present application, 10 meV energy resolution must be achieved at kinetic energies of several hundred eV. The analyzer pass energy will be approximately 1 eV, therefore, the lens system must provide a retardation ratio of several hundred. Such large acceleration / deceleration ratios cannot be properly achieved using simple two-element lenses (ref. 22). Depending on the parameters associated with the source and desired image, lenses having more than two elements are generally required to achieve good performance for deceleration ratios above 15. Recent analysis of four-element zoom lens systems (refs. 23-25) has shown that these lenses

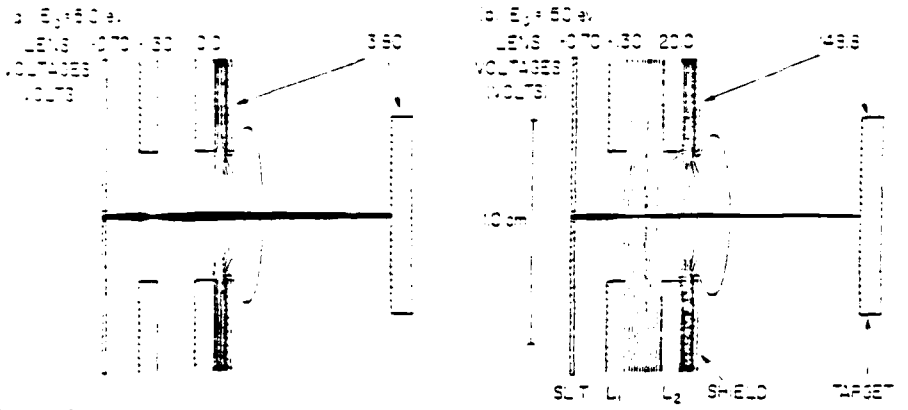

Figure 2. Ray tracing results for a common EELS lens system.

offer better performance and additional capabilities which cannot be achieved using two-element lenses or three-element zoom lenses. We have carried out extensive ray tracing studies and empirical tests of simple two-element lenses used in photoelectron emission spectroscopy (ref. 26) and in EELS optics (ref. 27), a three-element EELS lens system adapted for high impact energy studies of surface phonons (ref. 27), and of four-element zoom lenses (refs. 25,28) intended for use in the analyzer described by Figure 1.

Figure 2 illustrates an example based on a typical EELS lens system with operating voltages determined using the usual tuning procedure which maximizes intensity of the specular elastic peak scattered from the sample. This figure shows that ray tracing of a lens system based on lens voltages determined empirically appear to be the "correct " voltages as judged by the shape and focus positions of the electron beam determined by the ray analysis.

The primary result of these studies is that we have found that electron ray tracing analysis appears to yield accurate predictive results for voltages, electron trajectories and images for electron energies within the useful range of EELS applications (a few eV to beyond several hundred eV). This does not imply that high current monochromators can be designed based on conventional ray tracing. However, it does clearly demonstrate that ray tracing analysis can be effectively utilized in the design of monochromator acceleration optics where current densities are low, and in the analyzer deceleration optics. It will be quite feasible to obtain an accurate characterization of the analyzer transmission function using ray tracing and therefore to obtain accurate energy dependent EELS cross section data.

The tandem zoom lens configuration permits independent adjustment of the analyzer acceptance cone and the deceleration ratio. A similar design has been used by Kevan (ref. 29). The apertures A_1 and B_2 define a fixed area and solid angle for electrons entering the second zoom lens which functions as the deceleration stage. It is clear that a proper lens-apertures combination which provide effective control of the beam angular divergence as it enters the analyzer is very important in designs which utilize multichannel detection.

The first zoom lens is located near the scattering point and can be adjusted (within constraints set by the Helmholtz-Lagrange Law) to select the solid angle of detected electrons.

With elements of the first zoom lens grounded, A_1 and A_2 define a very small fixed acceptance angle for dipole scattering and LEED type measurements.

d. **Field Termination:** High resolution imaging detectors have been developed by several groups (refs. 30-33) and are also now available commercially (ref. 34). It is therefore relatively easy to improve the detection efficiency of suitably configured electron spectrometers by simply adding an array detector. This procedure is obviously more difficult for high resolution applications such as gas phase photoemission spectrometers and EELS analyzers than for ESCA analyzers; only a few successful implementations of multichannel detection in high resolution instruments have been reported. (refs. 7,35).

The primary difficulty in achieving high resolution with an analyzer which employs image detection is providing adequate field termination at the exit plane to preserve the images of individual energy channels. We have used electron ray tracing to investigate the perturbation of electron trajectories and the images formed at the exit plane of an analyzer having a channel plate detector biased at +150 volts relative to the two hemispheres. We used a model, illustrated in a previous paper, consisting of parallel plates having a one inch separation, and having applied voltages which simulate the electric field of the analyzer illustrated in Figure 1 operating at a 1eV pass energy. A 150 volt bias was applied to a conductor which simulated the channel plate in the model. The field terminator consisted of ten equally spaced tungsten ribbons having a 1 mil by 5 mil cross section and voltages applied to simulate the r^{-1} potential. A high transmission grid (~90%) biased at the entrance slit voltage is located immediately behind the ribbon array next to the channel plates. According to our ray tracing results, this configuration illustrated in Figure 1 should provide termination of stray fields adequate to achieve 5 meV energy resolution. Pollard et. al. (ref. 35) achieved 17 meV energy resolution in a multichannel detection gas phase photoelectron spectrometer based on a hemispherical analyzer having a mean radius of ~4 inches and operating at 2 eV pass energy. The channel plate field terminator used in this analyzer consisted of six concentric rings suitably biased to produce a piece-wise linear approximation of the potential. Ray tracing based on our simple model has accounted for this resolution and also shows that improved performance could have been achieved by adding additional concentric rings and a second grid biased at the central orbit potential as shown in Figure 1.

MONOCHROMATOR

Successful implementation of multichannel detection in an EELS spectrometer as outlined in the previous section offers good prospects of achieving a factor of 50-100 improvement in signal levels for applications now limited by very low counting rates (i.e., in experiments which rely on impact scattering). Corresponding improvements in monochromator performance appear to be much less likely to occur. Issues associated with achieving high energy resolution in high current monochromators have been dealt with by several investigators (refs. 36-38) and there are no strong indications of a means by which improvements can be achieved without a better fundamental understanding of the limiting factors. Significant improvements have been achieved in newer instruments by more effective coupling of the source and premonochromator to the entrance slit of

the main monochromator and by using larger energy dispersing elements (permitting larger slits and higher pass energies). Significant improvements may be possible by using a source which is based on photoemission from GaAs (ref. 39). At 30 meV resolution, the GaAs source provides over 10 times more current than that availabale from thermionic cathodes. However, additional evaluation is required to determine if this performance can be scaled to lower energy half widths.

CONCLUSION

An extensive feasibility study aimed at exploring the prospects of achieving significant improvements in EELS spectrometers has been carried out. The analysis has been based on a specific application involving inelastic scattering cross section measurements and surface phonon measurements which must rely on the weak impact scattering mechanism. Important results obtained by this work include the criteria for optimizing image quality (resolution) and flux (etendue) in a hemispherical analyzer which uses multichannel dection, criteria for choosing the optimium number of energy channels, and a suitable design for a high transmission field termination which perserves the image. In addition, extensive ray tracing analysis and empirical tests based on three different well characterized lens systems have established the predictive capabilities of ray tracing studies, even at low kinetic energies (i. e., 10 eV) which are common in EELS spectrometers used primarily for specular scattering (dipople scattering) studies. A prototype analyzer / monochromator EELS system has been constructed based on the results of the study and will be used to verify the model predictions and to explore impact scattering phenomena.

Acknowledgement: This work was sponsored by the Air Force Office of Scientific Research under Grant: AFOSR-83-0131.

REFERENCES

1. F. M. Propst and T. C. Piper, J. Vac. Sci. Technol. 4, 53 (1967).
2. H. Ibach, Phys. Rev. Letters 24, 1416 (1970); 27, 253 (1971).
3. Early review articles describe the development of EELS: for example refer to H. Froitzheim, Topics in Current Physics, ed. by H. Ibach (Springer-Verlag, New York 1976) Vol.4.
4. L. L. Kesmodel, J. Vac. Sci. Technol. A1, 1456 (1983).
5. R. L. Strong and J. L. Erskine, Rev. Sci. Instrum. 55, 1304 (1984).
6. S. Lehwald, J. M. Szeftel, H. Ibach, T. S. Rahman and D. L. Mills, Phys. Rev. Letters 50, 518 (1983).
7. R. Franchy and H. Ibach, Surf. Sci. 155, 15 (1985).
8. W. Ho, J. Vac. Sci. Technol. A3,1432 (1985).
9. S. D. Kevan and L. H. Dubois, Rev. Sci. Instrum. 55, 1604 (1984).
10. W. Goldammer, W. Ludwig, W. Zieran and C. Falter, Surf. Sci. 141, 139 (1984); W. Goldammer and W. Ludwig, J. de Phys. C5, 119 (1984).
11. D. C. Allen and E. J. Mele, Phys. Rev. Letters 53, 826 (1984).
12. R. L. Strong and J. L. Erskine, Phys. Rev. Letters 54, 346 (1985).
13. R. L. Strong and J. L. Erskine, Phys. Rev. B31, 6305 (1985).
14. J. M. Szeftel, S. Lehwald, H. Ibach, T. S. Raman, J. E. Black and D. L. Mills, Phys. Rev. Letters 51, 286 (1981).
15. G. Aers, J. B. Pendry, T. B. Grimley and K. L. Sebastian, J. Phys. C14, 3995 (1981).
16. B. M. Hall, S. Y. Tong and D. L. Mills, Phys. Rev. Letters 50, 1272 (1985).
17. M. L. Xu, B. M. Hall, S. Y. Tong, M. Rocca, H. Ibach S. Lehwald and J. E. Black, Phys. Rev. Letters 54, 1171 (1985).
18. W. Ho, R. F. Willis and E. W. Plummer, Phys. Rev. Letters 40, 1463 (1978); Phys. Rev. B21, 4202 (1980).

19. J. P. Woods and J. L. Erskine, Phys. Rev. Letters (in press).
20. H. Ibach and D. L. Mills, Electron Energy Loss Spectroscopy and Surface Vibrations, (Academic Press, New York 1982) Ch. 2.
21. F. Hadjarab and J. L. Erskine, J. Electron Spectrosc. Rel. Phenom. 36, 227 (1985).
22. C. E. Kuyatt, Electron Optics Lecture Notes, (1967). (widely circulated but unpublished)
23. G. Martinez and M. Sancho, J. Phys E: Sci. Instrum. 16, 625 (1983).
24. G. Martinez, M. Sancho and F. H. Read, J. Phys. E: Sci. Instrum. 16, 632 (1983).
25. A. K. Sellidj, M. A. Thesis, (1984), University of Texas, Austin.
26. H. A Stevens, A. W. Donoho, A. M. Turner and J. L. Erskine, J. Electron Spectrosc. Rel. Phenom. 32, 327 (1983).
27. R. L. Strong and J. L. Erskine, Rev. Sci. Instrum. 55, 1304 (1984).
28. A. K. Sellidj and J. L. Erskine (to be published).
29. S. D. Kevan, Rev. Sci. Instrum. 54, 1441 (1983).
30. W. Parkes, K. D. Evans and E. Mathieson, Nuclear Inst. Methods 121, 151 (1974).
31. M. Lampton and C. W. Carlson, Rev. Sci. Instrum. 50, 1093 (1979).
32. L. Mertz, T. D. Tarbell and A. Title, Appl. Optics 21, 628 (1982).
33. D. Rees, I. McWhirter, P. A. Rounce and F. E. Barlow, J. Phys. E: Sci. Instrum. 14, 229 (1981).
34. Surface Science Laboratories, Palo Alto, California.
35. J. E. Pollard, D. J. Trevor, Y. T. Lee and D. A. Shirley, Rev. Sci. Instrum. 52, 183 (1981).
36. C. E. Knyatt and J. A. Simpson, Rev. Sci. Instrum. 38, 103 (1967).
37. F. H. Read, J. Comer, R. E. Imhof, J. N. H. Brunt and E. Harting, J. Electron Spectrosc. Rel. Phenom. 4, 293 (1974).
38. H. Froitzheim, J. Electron Spectrosc. Rel. Phenom. 34, 11 (1984).
39. D. T. Pierce and R. J. Celotta (private communication).

END

DATE

FILMED

3-88

DTIC